Charles University in Prague
Faculty of Mathematics and Physics

MASTER THESIS

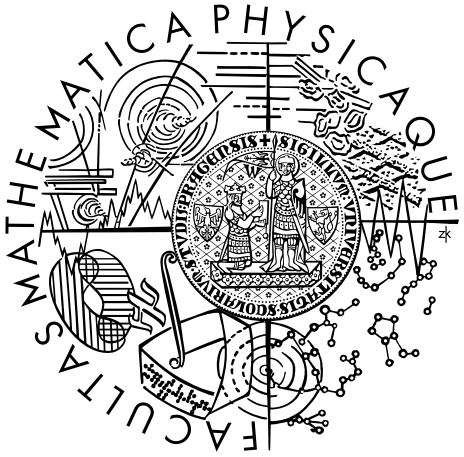

Jan Brandejs

Optimizing quantum simulations and the DMRG method

Department of Chemical Physics and Optics

Supervisor of the master thesis: doc. Dr. rer. nat. Jiří Pittner, DSc.

Study programme: Physics

Study branch: Theoretical Physics

Prague 2016

I declare that I carried out this master thesis independently, and only with the cited sources, literature and other professional sources.

I understand that my work relates to the rights and obligations under the Act No. 121/2000 Sb., the Copyright Act, as amended, in particular the fact that the Charles University in Prague has the right to conclude a license agreement on the use of this work as a school work pursuant to Section 60 subsection 1 of the Copyright Act.

In ..... date ..... signature of the author

Title: Optimizing quantum simulations and the DMRG method

Author: Jan Brandejs

Department: Department of Chemical Physics and Optics

Supervisor: doc. Dr. rer. nat. Jiří Pittner, DSc., J. Heyrovský Institute of Physical Chemistry of the Czech Academy of Sciences

Abstract: In this work, we explore the quantum information theoretical aspects of simulation of quantum systems on classical computers, in particular the many-electron strongly correlated wave functions. We describe a way how to reduce the amount of data required for storing the wavefunction by a lossy compression of quantum information. For this purpose, we describe the measures of quantum entanglement for the density matrix renormalization group method. We implement the computation of multi-site generalization of mutual information within the DMRG method and investigate entanglement patterns strongly correlated chemical systems. We present several ways how to optimize the ground state calculation in the DMRG method. The theoretical conclusions are supported by numerical simulations of the diborane molecule, exhibiting chemically interesting electronic structure, like the 3-centered 2-electron bonds. In the theoretical part, we give a brief introduction to the principles of the DRMG method. Then we explain the quantum informational motivation behind our quantum chemical calculations and present results.

Keywords: quantum simulation density matrix renormalization group quantum entanglement quantum information quantum chemistry

To Nature

Contents

Introduction and Motivation

"In the year 1992, S. R. White introduced a very powerful numerical method, the density-matrix renormalization group (DMRG). It allows us to determine the physical properties of low-dimensional correlated systems such as quantum spin chains or chains of interacting itinerant electrons to unprecedented accuracy." (from Szalay et al. [2015])// // Simulating quantum chemical problems is a well-known difficult task, whose complexity scales exponentially with the number of particles involved.

Since the quantum computers, promising an efficent solution to these problems have not arrived yet to practice, we must make use of the most powerful computing clusters in order to be able to simulate quantum chemistry. The electronic molecular Hamiltonian reads

$$\hat{H} = \hat{T} + \hat{U} \tag{1}$$

$$= -\sum_i \frac{\hbar^2}{2m_e}\nabla^2_{r_i} + \frac{1}{2}\sum_i \sum_{j>i} \frac{e^2}{4\pi\epsilon_0 |r_i - r_j|} \tag{2}$$

This would be impossible without using clever approximations and optimizations.

What do we mean by effective simulation? That is such simulation whitch exhibits polynomial scaling with the input size (e.g. number of particles, or more practically number of bytes).

There are many different methods which attemp to deal with the complexity of the quantum chemical simulations. Namely the density functional theory, coupled clusters, renormalization group methods and so on.

This thesis focuses on the density matrix renormalization group method from the quantum information theoretical point of view. We describe the DMRG optimizations and generalizations for multipartite entanglement calculations.

First we introduce the relevant quantum theoretical terms, then we explain how is the entanglement relevant for quantum chemical calculations. We explain the principles of some basic optimizations for the DMRG method and finally we conlude with describing the three-site mutual information calculation that we carried out for the diborane molecule, having programmed a new and fully general DMRG module for such calculations.

1. Quantum Entanglement and Quantum Information Theory

1.1 What is entanglement? Composite Quantum Systems

In this section, we will define the basic terms to clarify what do we mean by quantum entanglement and how do we think of the composite quantum systems from the viewpoint of Quantum Information Theory. Let us start with a definition of a pure state.

Definition 1 (Pure state)**.** *A quantum system is said to be in a pure state, if we, in theory, have a complete knowledge about the system. That is, we know exactly in which state the system is. In the Hilbert space $\mathcal{H}$, representing the possible states of a quantum system, the pure state is represented by a single vector $|\psi\rangle \in \mathcal{H}$.*

Let $\mathcal{H}$ be finite dimensional. That is, there is a finite set of basis states $|i\rangle \in \mathcal{H}$, such that each pure state in $\mathcal{H}$ can be expressed as

$$|\psi\rangle = \sum_{i=1}^{n} c_i |i\rangle , \; c_i \in \mathbb{C} \tag{1.1}$$

and we say $\mathcal{H}$ is n-dimensional.

Now we understand what is meant by a pure state. In contrast to the pure state, there is a mixed state, which we will define shortly. But first let's introduce the quantum entanglement.

Imagine a quantum system composed of two or more parts. From a mathematical point of view, such parts are the subspaces of full system's Hilbert space $\mathcal{H}$, which can be expressed as a tensor product of the subspaces. For a bipartite system built from partitions $\mathcal{H}_1$ and $\mathcal{H}_2$, we have $\mathcal{H} = \mathcal{H}_1 \bigotimes \mathcal{H}_2$. However, each state cannot be expressed as a tensor product $|\psi\rangle = |\psi_1\rangle \otimes |\psi_2\rangle$ of states from the first and second partition. To be exact, such states are the most common. So, how do we compose $|\psi\rangle$ from the subsystem states?

Let us fix the basis of $\mathcal{H}_1$ and $\mathcal{H}_2$ as $|j\rangle$ and $|k\rangle$, with a different dimension in general. Now each state $|\psi\rangle \in \mathcal{H}$ can be expressed a tensor product

$$|\psi\rangle = \sum_{j=1}^{n_1} \sum_{k=1}^{n_2} c_{jk} |j\rangle \otimes |k\rangle \tag{1.2}$$

where c_{jk} is a $n_1 \times n_2$ matrix of complex amplitudes. Further on, we will use a short notation $|j\rangle \otimes |k\rangle \equiv |j\rangle |k\rangle$. The above structure can be generalized to multiple partitions, with basis $|i_1\rangle |i_2\rangle |i_3\rangle ... |i_N\rangle$. Assuming all N partitions to have the same dimension q, the tensor of complex amplitutes then takes a form $c_{i_1 i_2 i_3 ... i_N}$, with a dimension q^N. This is the case for many-particle systems.

Now let's use the definition and examples from Galindo and Martín-Delgado [2002] to introduce the two key terms for this chapter.

Definition 2 (Entangled and separable state)**.** *A quantum pure state $|\psi\rangle$ in a Hilbert space $\mathcal{H} = \bigotimes_{i=1}^{N} \mathcal{H}_i$ is said to be separable with respect to the factor spaces $\mathcal{H}_1, ..., \mathcal{H}_N$, when it can be factorized as follows*

$$|\psi\rangle = \otimes_{i=1}^{N} |\psi_i\rangle \,, \; |\psi_i\rangle \in \mathcal{H}_i \tag{1.3}$$

Otherwise the state $|\psi\rangle$ is called entangled.

To give few examples of entangled states, we will use the simplest multipartite Hilbert space built of qubits, that is distinguishable spin-$\frac{1}{2}$ particles on the lattice, each such partition with dimension $q = 2$ and basis $|0\rangle, |1\rangle$. Here we will use common abbreviations like $|0\rangle \otimes |1\rangle \otimes |0\rangle \equiv |010\rangle$.

Famous examples are the Bell states or EPR pairs introduced by Einstein et al. [1935]

$$\left|\Phi^{\pm}\right\rangle := \frac{1}{\sqrt{2}} \left[|00\rangle \pm |11\rangle\right], \tag{1.4}$$

$$\left|\Psi^{\pm}\right\rangle := \frac{1}{\sqrt{2}} \left[|01\rangle \pm |10\rangle\right]. \tag{1.5}$$

According to Galindo and Martín-Delgado [2002], these states can be physically represented by a spin-$\frac{1}{2}$ triplet or singlet, or by entagled polarized photons.

For a three-qubit case, we will mention the GHZ state, introduced by Greenberger et al. [1989]

$$|\mathrm{GHZ}\rangle := \frac{1}{\sqrt{2}} \left[|000\rangle + |111\rangle\right]. \tag{1.6}$$

The GHZ state has been observed experimentally in polarization of three entangled spatially separated photons by Bouwmeester et al. [1999].

1.2 Measuring Entanglement

In past decades, it turned out that quantum entanglement is a feature that disctincts the quantum systems from classical ones. For instance, entanglement allows

quantum information to overcome some of the limitations posed by classical information, as exemplified by the phenomena of teleportation, dense coding, etc., to be explained in the following sections. For these reasons, a new view of entaglement had to be introduced by Bennett [1998], considering it a resource in quantum information. Something that we must have available if we want to exploit the new communication and cryptography possibilities offered by the quantum protocols.

And even if those futuristic concepts were not applied eventually, it is still essential to understand the qualification and quantification of quantum entanglement. Important questions like "How much is the system entangled?" gave rise to the *entanglement measures* and *separability criteria*, fields with still many unanswered questions and often without a consent over conclusions. These topics correspond to the issue of classification of multipartite entanglement, which have been explored for pure states, but for mixed state ensembles, there are still many open problems. In further text, we will discuss how various quantities measuring entanglement can be used for classifying the partial separability. We will show why these terms are relevant for optimizing the quantum simulations and how do we take advantage of them in designing the DMRG and other tensor product methods.

There are several types of entanglement measures that can be calculated from the density operator, which we will introduce shortly. Those entropies characterize the mixedness of a multipartite system state. Let us cite several examples given in the paper by Szalay et al. [2015]. The most commonly used entanglement measure is the von Neumann entropy, followed by the more general one-parameter Rényi entropies for parameter lower than 1, the Hartley entropy (assymptotically similat to Rényi entropy), the Schmidt rank, and the one-parameter family of Tsallis entropies.

Let us now briefly sum up the prerequisite definitions for intrucing some particular examples of the entanglement measures. First let us introduce the density operator. Assume a bipartite division of our quantum system in a state given by the equation (1.2). Then the reduced density matrix is defined based on the amplitudes of the state

$$\rho_{ij} \equiv \sum_{l} c_{il} c_{jl}, \tag{1.7}$$

where i and j index the basis states of the first subsystem, while the l indexex the second subsystem (environment), which we trace out. ρ_{ij} represents the matrix elements of the density operator $\hat{\rho}$.

$$\hat{\rho} \equiv \sum_{mn} |m\rangle \, \rho_{mn} \, \langle n| \tag{1.8}$$

which in turn represents the so called mixed state.

Now imagine a system composed of L identical sites of a 1D lattice. We may define the von Neumann entropy as.

Definition 3 (n-orbital entropy)**.** *Given an orbital labelled by index i on the lattice $i = 1 \dots L$, we define the one-orbital, two orbital and three orbital von Neumann entropy as*

$$S_i = -\sum_{\nu} \omega_{\nu i} \ln \omega_{\nu i}, \tag{1.9}$$

$$S_{ij} = -\sum_{\nu} \omega_{\nu ij} \ln \omega_{\nu ij}, \tag{1.10}$$

$$S_{ijk} = -\sum_{\nu} \omega_{\nu ijk} \ln \omega_{\nu ijk}, \tag{1.11}$$

$$\tag{1.12}$$

where $\omega_{\nu l}, \omega_{\nu ij}, \omega_{\nu ijk}$ are the eigenvalues of one-orbital, two-orbital and three–orbital reduced density matrix $\rho_i, \rho_{ij}, \rho_{ijk}$, indexed by ν, with the rest of the system traced out like in equation 3.2.

Now we are ready to define the site mutual information between two lattice sites.

$$I_{ij} = -S_{ij} + S_i + S_j. \tag{1.13}$$

This quantity is one of the most important entanglement measures and we will describe it further in chapter 3.

2. Matrix Product States and Tensor Product Approximation

2.1 Singular Value Decomposition

In this section, we will briefly introduce the priciple of *Singular Value Decomposition* (SVD), a very flexible tool from linear albegra widely used in the chapters to follow for entanglement based optimizations. This method, based on the good old separation of variables, provides us with a powerful framework for parametrizing tensors in a data-sparse representation suitable for quantum states in bipartite Hilbert spaces. In the case of quantum states, it is known as the *Schmidt decomposition*. Now we are going to define SVD, based on definition from the textbook by Golub and Van Loan [1996].

Figure 2.1: Singular Value Decomposition scheme. The figure shows dimensions of matrices in the equation (2.1). Left and right case correspond to $n_A \leq n_B$ and $n_A \geq n_B$ respectively. (from Schollwöck [2011])

Let $\mathcal{H}_A$ and $\mathcal{H}_B$ be the partitions (subspaces) of the system's Hilbert space $\mathcal{H}$. Now SVD states, that an arbitraty matrix M of dimensions $n_A \times n_B$ can be decomposed as

$$M = U D V^\dagger, \tag{2.1}$$

with

- U a $n_A \times n_{min}$, where $n_{min} \coloneqq \min n_A, n_B$ matrix with orthonormal columns, the so called *left singular vectors*, implying $U^\dagger U = I$. In the case when $n_A \leq n_B$, U becomes unitary with $UU^\dagger = I$.
- D is a diagonal $n_{min} \times n_{min}$ matrix with nonnegative diagonal entries d_i called the *singular values*. The number of nonzero singular values is the *Schmidt rank* of matrix M.

- $V^\dagger$ is a $n_{min} \times n_B$ matrix with orthonormal rows (the *right singular vectors*), with $V^\dagger V = I$. Analogically, when $n_A \geq n_B$, then also $VV^\dagger = I$ and V is unitary.

Remark. The number r of nonzero singular values is called the *Schmidt rank*. It is closely related to the *Schmidt decomposition* which we will describe shortly. Furthermore, it is straightforward that the bipartite quantum system is entagled (we say that the blocks are entangled) if and only if it's Schmidt rank is strictly greater than 1.

Remark. Note also that in certain cases when we are not particularly interested in the singular values, we can decompose M instead of $M = U D V^\dagger$ as $M = Q R$, with R playing the role of $D V^\dagger$. The so-called *QR decomposition* is faster to compute and retains the unitarity $QQ^\dagger = I$. Nevertheless for the DMRG method in further chapters, we will need to find the eigenvalues.

The mathematicians offer us an approximation based on SVD used widely in quantum chemistry. It approximates matrix M of rank r with a matrix M' of rank $m < r$. It optimizes chosen M' with respect to the so-called Frobenius norm $\|M'\|_F^2 = \sum_{ij} \left|M'_{ij}\right|^2$ induced by the scalar product $\langle A|B\rangle = \mathrm{Tr}\{A^\dagger B\}$. Let the singular values be sorted in descending order $d_1 \geq d_2 \geq ... \geq d_r$, then the optimal approximation M' is given by

$$M \approx M' \equiv U D' V^\dagger, \qquad D' = \mathrm{diag}\,(d_1,\, d_2,\, ...,\, d_r,\, 0, ...,\, 0)\,.$$

Thanks to SVD, we can shrink the column dimension of U and the row dimension of $V^\dagger$ to m in the quantum chemical computations.

We don't give a proof of the approximation here, since proof of a very similar statement for DMRG in dirac formalism can be found in the chapter 4.2. For a rigorous, but very readable proof of both SVD existence and the above approximation optimality, please refer to the mathematical lecture notes by Gander [2008].

2.2 The Principle of MPS

In this section, we introduce the *Matrix Product State*, one of the most effective methods for storing a quantum state in the computer memory, especially suitable for the many-body problems.

Let's have a Hilbert space built of many equal q-dimensional partitions. We will think of them as sites of a one dimensional lattice of length L. We can fix the basis for each site and label it e.g. $\{|i_1\rangle\}$, $i_1 = 1...q$ for site 1, $\{|i_2\rangle\}$ for site 2 and so on to L. We can write the general pure state as

$$|\psi\rangle = \sum_{i_1 \,...\, i_L} c_{i_1 \,...\, i_L} \,|i_1 \,...\, i_L\rangle\,, \tag{2.2}$$

with the number of coefficients $c_{i_1 \dots i_L}$ growing exponentially with respect to the number of lattice sites. We would like to find a representation of this state that is more local with respect to partitions, but at the same time preserves the nonclassical bonds between them. This can be done using the Singular Value Decompositin. We will see that even though the products may not seem to be very physical, they are closely connected to quantum theory.

Let us now follow the steps from Schollwöck [2011] to derive the procedure which decomposes the matrices from the left, resulting in the so-called *left-canonical MPS*. In order to put it in the SVD, we have to reshape the q^L-dimensional state vector into a $q \times q^{L-1}$ matrix by setting the first site to index the row number and other site indices to designate the column number. Then we perform the SVD, changing the basis $\{|i_1\rangle\} \mapsto \{|u_1\rangle\}$

$$\Psi_{i_1\,(i_2 \dots i_L)} = c_{i_1 \dots i_L} \tag{2.3}$$

$$\Psi_{i_1\,(i_2 \dots i_L)} = \sum_{u_1}^{r_1} U_{i_1 u_1} d_{u_1} V^{\dagger}_{u_1\ (i_2 \dots i_L)} \equiv \sum_{u_1}^{r_1} U_{i_1 u_1} c_{u_1\, i_2 \dots i_L}, \tag{2.4}$$

where in the last step (2.4), we multiplied D and $V^\dagger$ and reshaped it back into a vector c. Now the representation is a little bit more efficient, since the rank is now $r_1 \leq q$.

We proceed with an analogical procedure, just for the second lattice site index. We decompose $U_{i_1 u_1}$ into q row vectors A^{i_1} with elements $A^{i_1}_{u_1} = U_{i_1 u_1}$. In order to be able to use SVD again, we also have to reshape $c_{u_1\, i_2 \dots i_L i} \longmapsto \Psi_{(u_1\, i_2)\,(i_3 \dots i_L)}$. So Ψ is a rectangular matrix with dimension $r_1 q \times q^{L-2}$. Altogether, this yields following form of c, where we apply the SVD to Ψ in the second step

$$c_{i_1 \dots i_L} = \sum_{u_1}^{r_1} A^{i_1}_{u_1} \Psi_{(u_1\, i_2)\,(i_3 \dots i_L)}, \tag{2.5}$$

$$\begin{aligned} c_{i_1 \dots i_L} &= \sum_{u_1}^{r_1} \sum_{u_2}^{r_2} A^{i_1}_{u_1} U_{(u_1\, i_2)\, u_2}\, d_{u_2} V^{\dagger}_{u_2\ (i_2 \dots i_L)}, \\ &= \sum_{u_1}^{r_1} \sum_{u_2}^{r_2} A^{i_1}_{u_1}\, A^{i_2}_{u_1\, u_2} \Psi_{(u_2\, i_3)\,(i_4 \dots i_L)}, \end{aligned} \tag{2.6}$$

with another reshape-reorder $U_{(u_1\, i_2)\, u_2} \longmapsto A^{i_2}_{u_1\, u_2}$ and a multiplication $d_{u_2} V^{\dagger}_{u_2\ (i_2 \dots i_L)} \longmapsto \Psi_{(u_2\, i_3)\,(i_4 \dots i_L)}$. Note the possible decrease of number of elements to be kept $r_2 \leq r_1 q \leq q^2$, where we refer to the dimensions of Ψ, which is now $r_2 q \times q^{L-3}$. To be complete, we add that A^{i_2} is a $r_1 \times r_2$ matrix. In analogy to the previous two iterations, we continue with applying SVDs and reshaping to arrive

to the equality

$$\begin{aligned} c_{i_1 \dots i_L} &= \sum_{u_1 \dots u_L} A^{i_1}_{u_1} A^{i_2}_{u_1\, u_2} \dots A^{i_{L-1}}_{u_{L-2}\, u_{L-1}} A^{i_L}_{u_{L-1}} \\ &\equiv A^{i_1} A^{i_2} \dots A^{i_{L-1}} A^{i_L}, \end{aligned} \tag{2.7}$$

where we wrote the last expression in a compact notation of the matrix product. Note that A^{i_1} and A^{i_L} are vectors, but we can make them matrices by appending a dummy index. Then we can write our quantum state as a *matrix product state*

$$|\psi\rangle = \sum_{i_1 \dots i_L} A^{i_1} A^{i_2} \dots A^{i_{L-1}} A^{i_L} \, |i_1 \dots i_L\rangle \, . \tag{2.8}$$

To be able to perform this procedure on the computer, we have to revise the dimensions of A-matrices. The maximum dimension will be reached when for each SVD, the number of non-zero singular values equals the upper bond. Counting the above SVD iterations, we obtain following dimensions of A-matrices: $1 \times q$, $q \times q^2$, ..., $q^{L/2-1} \times q^{L/2}$, $q^{L/2} \times q^{L/2-1}$, ..., $q^2 \times q$, $q \times 1$, going from the first to the last site. In the middle of the lattice, the matrix dimension blows up exponentially. Thus it is usually impossible to decompose a many-body quantum state to the exact MPS representation. We have to introduce some approximations.

We will see in following chapters that the MPS form is particularly appropriate for the approximations of many-body systems in quantum chemistry and solid state physics.

Remark. Note another usefull feature of the A-matrices. For each SVD above, $U^\dagger U = I$ holds. After a substition of U with a sequence of A^i, we see that

$$\begin{aligned} \delta_{u_m\, u_n} &= \sum_{u_{m-1}\, i_m} U^\dagger_{u_m\, (u_{m-1}\, i_m)} U_{(u_{m-1}\, i_m)\, u_n} \\ &= \sum_{u_{m-1}\, i_m} A^{i_m \dagger}_{u_m\, u_{m-1}} A^{i_m}_{u_{m-1}\, u_m} \\ \Rightarrow \; &\sum_{i_m} A^{i_m \dagger} A^{i_m} = I \end{aligned} \tag{2.9}$$

Such matrices are called *left-normalized* and a matrix product state will all matrices left normalized is being refered to as *left-canonical*. Equation (2.9) may not hold for the last site, but that's just a minor technicality.

Remark. There was nothing special on starting from the first site on the left. We can also carry out an analogical procedure starting from the last site and proceeding in the opposite order. The result is then called *right-canonical matrix product state* and its matrices are *right-normalized*.

Consider also combining the two procedures, starting with the decomposition from the left, reaching lattice site l and then continuing with the decomposition from the right, finishing at l. This approach yields the so called *mixed-canonical matrix product state*, decomposing the tensor c from equation (2.2) as

$$c_{i_1 \dots i_L} = A^{i_1} \dots A^{i_l} \, D \, B^{i_{l+1}} \dots B^{i_L}, \tag{2.10}$$

where B^i are the matrices of the decomposition from the right and D is a diagonal matrix of singular values of the bond $(l,\ l+1)$.

This form of MPS is particularly interesting for its correspondence with the decomposition in the DMRG method in chapter 4.3.

For further details about the different approaches to MPS decomposition, please refer to Schollwöck [2011].

Remark. The MPS can be used even for multi-dimesional lattices and for those the presented derivation holds too. The problem is that the numerical treatment of states based on a multi-dimensional lattice is very demanding in terms of the computational resources. Multi-dimensional version of MPS representation is called *Tree Tensor Network State* . For futher reference please see Szalay et al. [2015].

Remark. The MPS decomposition is not unique! There is a freedom in choosing the gauge. Let's have two adjacent sets of matrices M^{i_l}, $M^{i_{l+1}}$, such that they can be multiplied, with the multiplication row/column dimension D. The matrix product state is invariant under a following transformation by a $D \times D$ matrix X

$$M^{i_l} \longmapsto M^{i_l} X, \qquad\qquad M^{i_{l+1}} \longmapsto X^{-1} M^{i_{l+1}}. \tag{2.11}$$

This fact gives the decomposition a gauge degree of freedom.

3. Optimizing Quantum Chemical Ab initio Calculations

When dealing with the quantum chemical problems described in the Introduction, we need to employ a number of approximations, and clever wavefuction representations in order to overcome the exponential complexity scaling for many-body problems. We will see in this chapter, that quantum information theoretical framework may offer some important approaches to treat the system more effectively. The related matrix product state formalism which was introduced in the previous chapter proves to be extremely handy in these applications.

3.1 Using Entanglement for Optimization and Classification

3.1.1 The Role and Significance of Entanglement

Entangled quantum systems exhibit a behaviour completely different from classical systems. The observed phenomena have no classical counterpart and in this sense we approach entirely new branch of physics. Entanglement is one of the most important, if not the most important feature determining the "quantumness" of a physical system. As was shown by Bell [1964], quantum entanglement is not a negligible, unimportant property of the system. It can strongly influence the system and it can easily have a deep impact on the system behaviour, especially for cats (see Schrödinger [1935]) and more importantly for the discussed fields of quantum chemistry and solid state physics (see the review by Szalay et al. [2015]).

There are several effective methods for simulating strongly correlated chemical systems. One of these is the *Density Matrix Renormalization Group* (QC-DMRG), which we will describe quite extensively in this work. This method uses the entanglement knowledge itself to effectively aproximate systems of many orbitals connected with potentially a large number of pairwise interactions.

Entanglement related concepts have been successfully used by quantum information theorists to explain the criteria of convergence of this group of numerical methods. On top of that, the quantum information theory contributed notably in chemistry, to the development of the electronic structure theory.

In this chapter, we will examine how can the quantum information theory findings contribute to quantum chemical calculations. What new does it tell us about the structure of the chemically interesting systems, how can we use it to optimize the necessary approximations, or even to design a completely new methods based

on the quantum correlations knowledge.

For instance, we can characterize the amount of correlation of an orbital with the rest of the system by the *single-orbital entropy*. Sum of these entropies for all orbitals gives a *total correlation*, which we can use to detect changes in the entanglement structure when we modify our representation of wavefunction or when we alter the system parameters like bond lengths, geometry etc.

However, *mutual information* is the most important quantity brought by the Quantum Information theory. It can be used to characterize the entanglement structure of our system. If we calculate it, then theoreticaly, without any previous knowledge of the system, we are able to find the most important bonds between orbitals, to describe the molecule topology, or to detect or verify the presence of a specific chemical bond between two arbitraty subsystems in any basis we choose (see Nalewajski [2004] and Szalay et al. [2016]). Also, it provides a good estimate of the complexity for methods designed to cope with the strongly correlated systems, e.g. the QC-DMRG, since they are widely dependent on the amount of correlation present (see Szalay et al. [2015]). We will show in section 4.4 that mutual information can be used in the numerical simulations as a cost function for optimizing the basis and topology of our reprentation, and for the efficient initialization of the computation.

3.1.2 Schmidt Decomposition

We have already mentioned that there is a very important application of SVD for quantum chemistry, called the *Schmidt Decomposition*. Let us now explain its principle with the quantum chemistry in mind. We will show how the Schmidt Decomposition can be used for any quantum state. A *pure* quantum state of a bipartite system AB can be written as

$$|\psi\rangle = \sum_{i,j} \Psi_{ij} |i\rangle |j\rangle , \tag{3.1}$$

where $|i\rangle$ and $|j\rangle$ are the orthonormal single-partition bases of A and B. The reduced density operators and their respective matrix forms are defined as

$$\begin{aligned} \hat{\rho}_A &= \mathrm{Tr}_B |\psi\rangle \langle\psi| & \hat{\rho}_B &= \mathrm{Tr}_A |\psi\rangle \langle\psi| \\ \rho_A &= \Psi\Psi^\dagger & \rho_B &= \Psi^\dagger\Psi. \end{aligned}$$

Setting n_{min} to be the dimension of the smaller partition, we are ready to employ the SVD on the density matrix Ψ in equation (3.1) in order to obtain a

sum

$$\begin{aligned}|\psi\rangle &= \sum_{ij}\sum_{k=1}^{n_{min}} U_{ik}D_{kk}V_{jk}\,|i\rangle\,|j\rangle \\ &= \sum_{k=1}^{n_{min}}\left(\sum_i U_{ik}\,|i\rangle\right) d_k \left(\sum_j V_{jk}\,|j\rangle\right) \\ &= \sum_{k=1}^{n_{min}} d_k \left|u^k\right\rangle_A \left|u^k\right\rangle_B . \end{aligned} \tag{3.2}$$

Thanks to the above declared orthonormality of U and $V^\dagger$, single-partition bases $\left|u^k\right\rangle_A$ and $\left|u^k\right\rangle_B$ are both orthogonal and span subspaces of the full partitions A and B respectively. Restraining ourselves to the sum over only the r nonzero singular values, we arrive to the final result, the *Schmidt Decomposition*

$$|\psi\rangle \equiv \sum_{k=1}^{r} d_k \left|u^k\right\rangle_A \left|u^k\right\rangle_B . \tag{3.3}$$

Remark. Note that the squares of the *Schmidt values* are exactly the density matrix ρ_A eigenvalues.

We can use the Schmidt decomposition for approximating the system's wave function by limiting the number of eigenstates in the sum (3.3) to certain number m. We will see in chapter 4 how does it work and why is it a very appropriate method for strongly correlated quantum chemical systems.

3.1.3 Block Entropy, Multiple Site Correlations and Mutual Information

In the quantum chemical methods in our focus, we will usually divide the full many-body Hilbert space into a number of smaller subspaces. Those will consist of one or few neighbouring orbitals. In order to analyse the interactions of the subspaces and the bonding within, we can observe the change of von Neumann entropy of this block with respect to its size.

It can even be used to study the quantum phases of one-dimensional systems. In the paper of Szalay et al. [2015], the behaviour of block entropy for one dimensional critical system with soft modes is simulated. On figure 3.1, we can see that the entropy oscillates with enlarging the block by adding more orbitals. This behaviour is caused by grouping of orbitals into more entangled clusters. When we add just a part of such cluster in our block, it will result in increase of block entropy, reflecting the bonds of the block with the rest of the system.

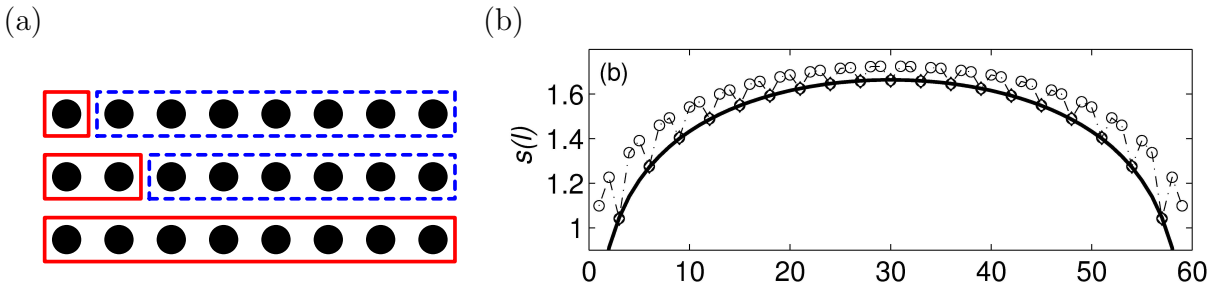

Figure 3.1: (a) Scheme of a contiguous block of lattice orbitals to determine block entropy. (b) Profile of block entropy computed via the DMRG method for critical one-dimensional model with soft modes. (from Szalay et al. [2015])

This was for a system with only local interactions. When the nonlocal interactions are present, the entropy behaviour becomes more complex. As we can see on the figure 3.2, the curve is strongly dependent on the order in which we add the system's orbitals to our block. We will use this fact later on for optimizing the ordering of orbitals in our DMRG simulation.

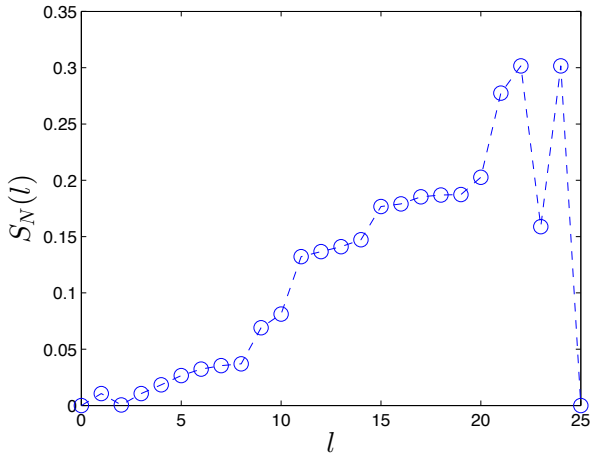

Figure 3.2: Block entropy profile calculated using the DMRG method for LiF molecule. Nonlocal interactions present in this system are responsible for complex shape of the curve. (from Szalay et al. [2015])

We have mentioned earlier in section 3.1.1, that the *single-orbital entropy* and the *mutual information* can be used for describing certain features of chemical systems. Let us now define those quantities in the quantum chemical terms.

First we will discuss the *single-orbital entropy*. It's value is related to the mixedness of a local state as it is expressed by the eigenvalues of the one-orbital

reduced density matrix.

It was shown by Legeza and Sólyom [2003], that the closer the orbital is to the *Fermi surface*, the larger is magnitude of the single-orbital entropy. The value of th one-orbital entropy is important, because, we can deduce the amount of contribution of the orbital to the total correlation energy. See figure 3.3 for an example plot of single-orbital entropy of the LiF molecule.

Summing up the single-orbital entropies yields the *total correlation* of the system, defined as

$$I_{tot} = -\sum_{l=1}^{L} S_l. \tag{3.4}$$

We can assume that the full system is in the pure state, then this sum gives us an information on how much entanglement is encoded in the wave function - it is equal to *total entanglement*.

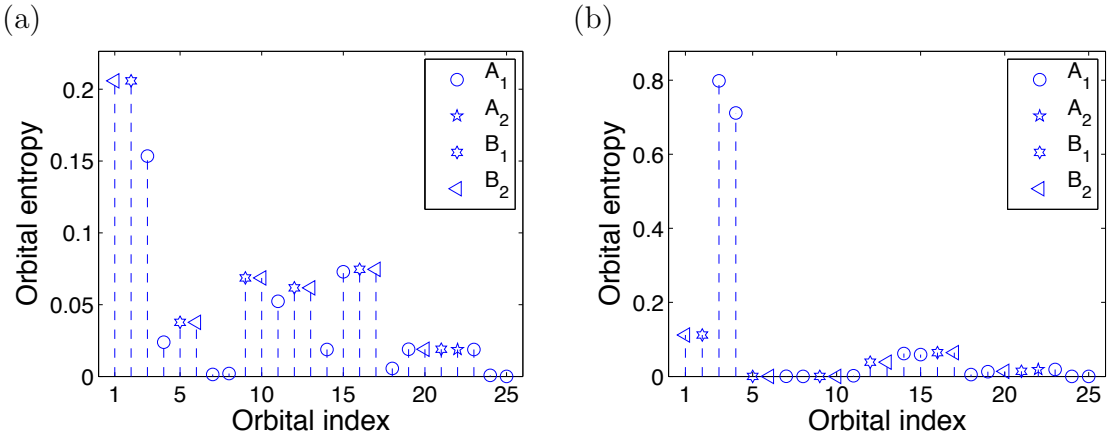

Figure 3.3: Single orbital entropy profiles for LiF molecule at different bond lengths. (a) $d = 3.05$ a.u. (b) $d = 13.7$ a.u.. Symbols indicate the irreducible represantantions of orbitals in the point group C_{2v}. (from Szalay et al. [2015])

Changing the parameters of the system will induce a change in total correlation. We can use it to watch how much did the system's entanglement pattern change upon a modification. This modification doesn't have to be as significant as changing the topology of the system, it is clear from figure 3.3 that even a slight change of bond-length may strongly influence both the total correlation and the single-orbital correlations.

The most important among those quantities is the *mutual information*, which has been defined in section 1.2. For two orbitals, it reads

$$I_{ij} = -S_{ij} + S_i + S_j. \tag{3.5}$$

This is the total correlation between the orbitals i and j. S_{ij} here is the von Neumann entropy of the subsystem consisting of the two orbitals. In general, both classical and quantum correlations contribute to I_{ij}.

It can be used to study molecular bonding properties of various quantum chemical or solid state systems, e.g. spin or fermionic chains, metal complexes etc. We can exploit this information for omptimization of our representation of the wave function, i.e. modify its structure to reflect the entanglement pattern given by the two-orbital mutual information plot. As shown in Legeza et al. [2008], respecting the system's entanglement structure may be of vital importance to the complexity of our simulation.

On figure 3.4 see example plot of two site mutual information, where we see how the entanglement structure depends on the the system parameters. Note that the relevant correlations stay even after this change.

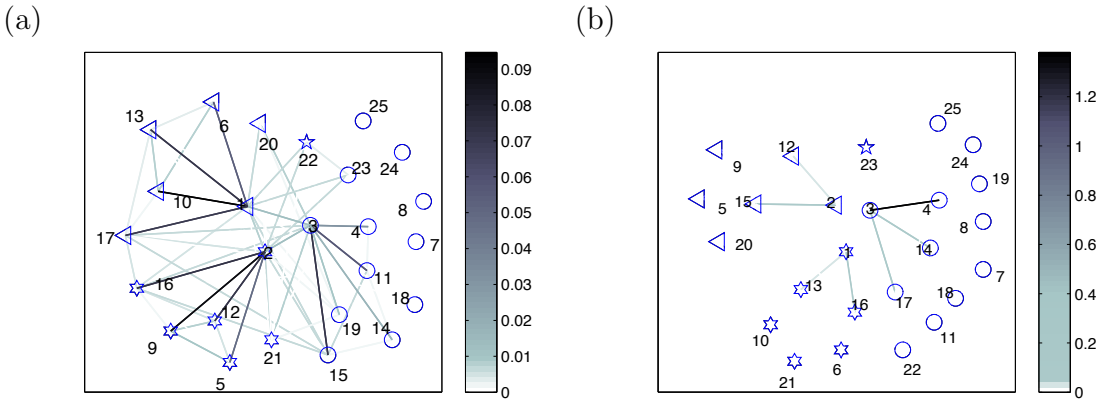

Figure 3.4: Change of entanglement pattern with respect to the bond length for the LiF molecule. (a) $d = 3.05$ a.u. (b) $d = 13.7$ a.u.. Same as on the figure 3.3, symbols indicate the irreducible represantantions of orbitals in the point group C_{2v}. (from Szalay et al. [2015])

We can extend these thoughts to even more orbitals. In general, we could use n-orbital reduced density matrix to define the mutual information between n-orbitals. However, this quantity is usually not considered relevant for higher n, since the amount of correlation tends to vanish exponentially with n. Also, according to Barcza et al. [2015], for $n > 2$, the relevant measures of correlations and their interpretations are not fully understood yet, and the structure of entanglement can ve very complicated. In the simplest $n = 3$ three-orbital case, the mutual information is usually defined as a generalization of two-orbital case, based

on Venn diagrams,

$$\begin{aligned} I_{ijk} =& S(\rho_{ijk}) - S(\rho_{ij}) - S(\rho_{ik}) - S(\rho_{jk}) \\ &+ S(\rho_i) + S(\rho_j) + S(\rho_k) \end{aligned} \tag{3.6}$$

where S is the von Neumann entropy. We will mention the three-orbital mutual information often in the following chapters, since calculating it was the main objective of a practical part of this thesis.

The above quantities provide us with chemical information about the system, in particular about the bond formation. Also thanks to these quantities, it is possible to explain the nature of static and dynamic correlations in the system.

3.1.4 Reduced Density Matrix: Generalized Correlation Functions

Another approach to studying the entanglement encoded in the mutual information is to analyze the matrix elements of two-orbital reduced density matrix ρ_{ij}. We will present now a practical way to calculate the two-orbital and also n-site mutual information.

Having the usual L-site wavefunction

$$|\psi\rangle = \sum_{u_1 \dots u_L} c_{u_1 \dots u_L} |u_1\rangle \dots |u_L\rangle , \tag{3.7}$$

with the tensor of coefficients $c_{u_1 \dots u_L}$, we can calculate the two-site reduced density matrix ρ_{ij} by taking the partial trace in $|\psi\rangle\langle\psi|$ over all indices of local bases except for u_i and u_j

$$\rho_{ij} = \sum_{\substack{u_k, u'_k \\ \forall k \neq i,j}} c^{\star}_{u'_1 \dots u'_L} c_{u_1 \dots u_L}. \tag{3.8}$$

Here each ρ_{ij} has still four indices u'_i, u'_j, u_i, u_j, which we pair up as (u'_i, u'_j), (u_i, u_j), in the sense that each pair labels a basis state of the two-site subsystem ij. Now ρ_{ij} is really a matrix with dimension $q^2 \times q^2$. Its single matrix element $(\rho_{ij})_{u'_i u'_j u_i u_j}$ corresponds to the transition $|u_i\, u_j\rangle \mapsto |u'_i\, u'_j\rangle$ between the basis states of subsystem ij, which also has dimension q^2.

Let me pause for a while to emphasize that we this correspondence will soon provide us with a practical way how to calculate the ρ_{ij} matrix elements. But before describing it, we will show how to calculate ρ_{ij} from the matrix product state form.

The dimension of $c_{u_1 \dots u_L}$ grows exponentially with the number of sites L. So calculating ρ_{ij} like this is practically impossible from many-body systems. Fortunately, for most chemically interesting systems, there exists a decomposition in

the form of a product of matrices

$$|\psi\rangle = \sum_{u_1 \dots u_L} A^{u_1} A^{u_2} \dots A^{u_{L-1}} A^{u_L} \, |u_1 \dots u_L\rangle \,, \tag{3.9}$$

which we derive in section 2.2 and which we can use for a more compact and approximated representation of $|\psi\rangle$. Having the state in matrix product form, calculation of ρ_{ij} now corresponds to the contraction of the tensor network $A^{\star u'_1} \dots A^{\star u'_L} A^{u_1} \dots A^{u_L}$ over all pairs of indices u'_k, u_k except i and j

$$\rho_{ij} = \sum_{\substack{u_k,\, u'_k \\ \forall k \neq i,\, j}} A^{\star u'_1} \dots A^{\star u'_L} A^{u_1} \dots A^{u_L}, \tag{3.10}$$

which you can see also schematically on figure 3.5. So if we have the MPS form of $|\psi\rangle$, we have a straightforward way to calculate the ρ_{ij}.

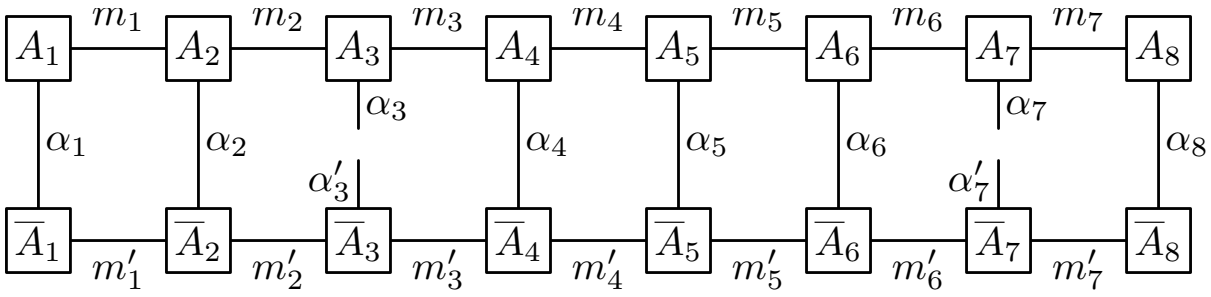

Figure 3.5: Contraction of the MPS network for calculating the two-site reduced density matrix ρ_{ij} for $i = 3$, $j = 7$ a lattice with 8 orbitals. Connected lines correspond to the contraction of indices, whereas the four lines without connection to any A_i represent the four free indices of ρ_{ij}. (from Szalay et al. [2015])

A slightly different approach which we applied in our practical calculations is to make use of the following relation for the density operator which expresses the correspondence emphasized above

$$\hat{\rho}_{ij} = \sum_{u'_i\, u'_j\, u_i\, u_j} (\rho_{ij})_{u'_i\, u'_j\, u_i\, u_j} \, \left|u'_i\, u'_j\right\rangle \langle u_i\, u_j| \,. \tag{3.11}$$

In this equation, we can see explicitly the correspondence of matrix elements of ρ_{ij} with transition amplitudes between the basis states of subspace ij. It becomes clear that we can calculate the matrix elements of ρ_{ij} as the expectation values of transition operators

$$(\rho_{ij})_{u'_i\, u'_j\, u_i\, u_j} = \langle\psi| \, T^{(u'_i\, u'_j)}_{(u_i\, u_j)} \, |\psi\rangle \tag{3.12}$$

and that's exactly how we calculated ρ_{ij} in the practical part. Just to clarify, here the operator $T^{(u'_i\,u'_j)}_{(u_i\,u_j)}$ corresponds to the transition $|u_i\,u_j\rangle \mapsto \left|u'_i\,u'_j\right\rangle$. The matrix elements of this operator are really simple: zeroes everywhere, except for a single 1 at row $(u'_i\,u'_j)$, column $(u_i\,u_j)$. The expectation values $\langle\psi|\,T^{(u'_i\,u'_j)}_{(u_i\,u_j)}\,|\psi\rangle$ are usually refered to as the *two-site generalized correlation functions* (see Barcza et al. [2015]).

We can also consider the simpler one-site case, where in equation (3.8), we don't leave out two pairs of indices, but just one pair, getting ρ_i. Analogically we define the one-site basis transition operators, calculate their expectaion values $\langle\psi|\,T^{u'_i}_{u_i}\,|\psi\rangle$ to obtain the elements of the *one-site reduced density matrix*.

Note that we can express the two-site transition operators in terms of those single-site transitions as

$$T^{(u'_i\,u'_j)}_{(u_i\,u_j)} = T^{u'_i}_{u_i}\,T^{u'_j}_{u_j} \tag{3.13}$$

$$= \bigotimes_{k=1}^{i-1} \mathbb{1} \otimes\; T^{i'}_{i} \bigotimes_{k'=1}^{j-i-1} \mathbb{1} \otimes\; T^{j'}_{j} \bigotimes_{k''=1}^{L-j} \mathbb{1}, \tag{3.14}$$

where without loss of generality $i < j$. The second equality holds when all the lattice sites are equal q-dimensional subspaces of the full Hilbert space, thus we can define a transition operator $T^{i'}_{i}$ between single-site basis states i and i'. For this case, assuming that the local states are completely distinguished by abelian quantum numbers, e.g. the one-site reduced density matrix can be calculated like

$$\rho_i \;=\; \langle\psi|\begin{bmatrix} T^{1_i}_{1_i} & 0 & 0 & \dots & 0 \\ 0 & T^{2_i}_{2_i} & 0 & \dots & 0 \\ \vdots & \vdots & \vdots & \ddots & \vdots \\ 0 & 0 & 0 & \dots & T^{q_i}_{q_i} \end{bmatrix}|\psi\rangle \tag{3.15}$$

The above two-site reduced density matrix calculation can be generalized to the three-site version

$$(\rho_{ij})_{u'_i\,u'_j\,u_i\,u_j} = \langle\psi|\,T^{(u'_i\,u'_j)}_{(u_i\,u_j)}\,|\psi\rangle \tag{3.16}$$

$$(\rho_{ijk})_{u'_i\,u'_j\,u'_k\,u_i\,u_j\,u_k} = \langle\psi|\,T^{(u'_i\,u'_j\,u'_k)}_{(u_i\,u_j,u_k)}\,|\psi\rangle\,, \tag{3.17}$$

where $T^{(u'_i\,u'_j\,u'_k)}_{(u_i\,u_j,u_k)}$ operates in the q^3 dimensional subspace formed by the three lattice sites ijk. It represents the transition $|u_i\,u_j\,u_k\rangle \mapsto \left|u'_i\,u'_j\,u'_k\right\rangle$ in this subspace. The indices of ρ_{ijk} are again grouped as $(u_i\,u_j\,u_k)$ and $(u'_i\,u'_j\,u'_k)$ so that ρ_{ijk} is a $q^3 \times q^3$ matrix for a single ijk combination. There is L^3 of ijk combinations, so the amount of data is growing considerably and we have to think of sparse matrix data representation and other tricks to be able to work with it.

To calculate the mutual information, first we have to calculate the von Neumann entropy of the subsystem described by reduced density matrix ρ. That is $S(\rho) = \mathrm{Tr}\{\rho \ln \rho\}$. If we know the eigenvalues ω_ν of ρ, this calculation simplifies to $S(\rho) = \sum_\nu \omega_\nu \ln \omega_\nu$. Then we are free to use the equations (3.5) and (3.6) to calculate the two-site and three-site mutual information I_{ij} and I_{ijk}.

This is enough for introducing the *generalized correlation functions* and explaining how to form the reduced density matrix from them. It may seem simple, however calculating these expectation values is not so easy in practice. The reason for this is because it's impossible to store the full form of quantum operators and quantum states in the classical computer. We will explain further in chapter 5 how we dealt with it for large many-body states.

3.2 Selected Methods in Matrix Product States language

In this section, we will describe few methods compatible with MPS state representation. The main goal is to decribe a historical path that led to the developmnet of the DMRG method, that we use in our calculations.

3.2.1 Block Renormalization Group Method

The *Block Renormalization Group Method* (BRG) was introduced by Kadanoff [1966] for the two-dimensional Ising model. Kadanoff attempted to approximate the full configuration Hilbert space of a L-orbital system. Later it was applied also to one-dimensional quantum systems.

The idea behind of this method is to group the orbitals into blockso of size l. The Hamiltonian is then divided into a part corresponding to the *intrablock* interactions between the orbitals inside the block and *interblock* interactions between the blocks. The full Hamiltonian is then a sum of many *interblock* and *intrablock* terms. In each iteration we pick the m lowest lying eigenstates of the intrablock subsystem and truncate the rest, transforming each Hamiltonian into a new form in the new approximated basis.

So the new basis is determined only with respect to the truncation in intrablock subspace. This truncation then propagates into the rest of the operators. Thanks to keeping only m states per block, we can rescale the interactions strengths (flow equations) and retain the original form of the full Hamiltonian.

In the following iteration, we take the blocks and join them together in groups of l. From each the big block, we again keep only m lowest eigenstates of the intrablock Hamiltonian. In this way we continue on and on, each time joining l blocks into one larger block and truncating it. The scheme of connecting sites

into blocks is on the figure 3.6. This procedure we repeat until we reach the *fixed point*, that is, the iterations stop changing the interaction strenths. Then we can calculate the physical quantities in the limit $\to \infty$.

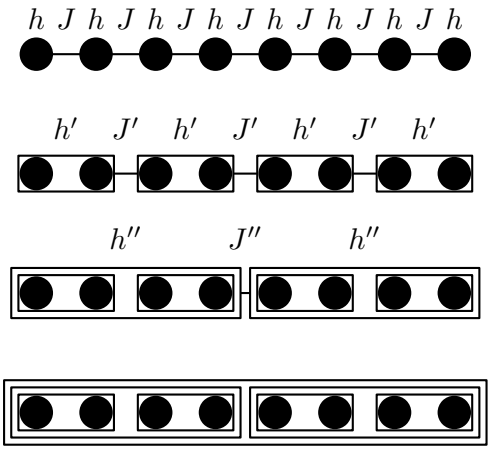

Figure 3.6: Scheme of forming the block in the Block Renormalization Group method. J labels nearest neighbor interaction and h denotes on-orbital interaction. (from Szalay et al. [2015])

Unfortunately, this procedure truncates the system so dramatically, that it can't be used in the quantum chemistry. The strongly entangled systems with long range interacions loose their essential correlation structures, even though there have been some recent developments succesfully altering this method in favour of such systems (see Szalay et al. [2015]).

3.2.2 Numerical Renormalization Group Method

Another method based on BRG which was to fix its problems is called the *Numerical Renormalization Group Method* (NRG). It was developed by Wilson [1975]. Wilson considered an impurity on the one-dimensional lattice, interacting with a local fermion. The exited states of this fermion live in the semi-infinite latttice with an impurity sitting on the first site. The system has exponentially decaying probability of hopping into the higher excited states with hopping amplitude $\lambda^{-l/2}$. This one-dimensional network is called the *Wilson chain*.

We start with a small block of 1 orbital. Then in each iteration, we enlarge it by adding one lattice site, diagonalize the Hamiltonian of the system and perform truncation, keeping only m lowest lying eigenstates. The new intrablock Hamiltonian is rescaled to reflect the decaying amplitudes of the hopping of its excited eigenstates. See figure 3.7 for the scheme of enlarging the block.

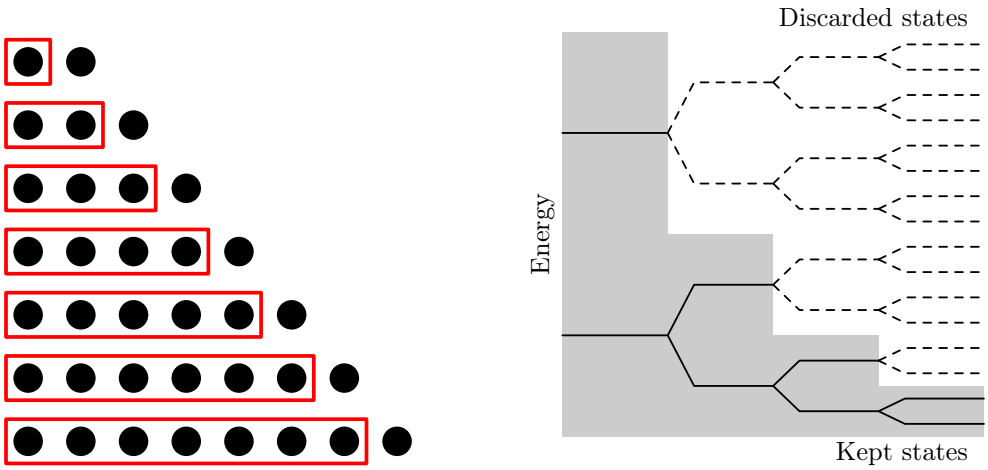

Figure 3.7: Scheme of forming the block in the Numerical Renormalization Group method. On the left, the block decimization procedure is depicted. On the right we can see how the high energy states are discarded, leading to exponential refinement of the NRG energy resolution. (from Szalay et al. [2015])

In this method, only $q < m < L$ states are kept, making it impossible to retain the original form of Hamiltonian. Also the flow equations cannot be studied in this approach. This method also stops at the*fixed pont*, when the subsequent interations leave the energy spectrum unchanged.

The whole method works thanks to the separation of energy eigenstates. However, for the systems in which the factor $\lambda \to 1$, we are getting into trouble with amplitudes not decaying quickly enough and the truncation error accumulates promptly (see Szalay et al. [2015] or Wilson [1975]). Thus for large models, the applications may be very problematic and plagued by errors.

3.2.3 Density Matrix Renormalization Group

Fortunately, there is another method which solves problems of both BRG and NRG. It's name is the *Density Matrix Renormalization Group* (DMRG) and it was developed by Wilson [1975]. It incorporates a more sophisticated way of truncating the states, based on the Singular Value Decomposition, working with the eigenstates of the reduced density matrix, instead of the Hamiltonian directly. The idea is to focus on minimizing the error of approximation of the wave-function of subsystem described by the "intrablock" reduced density matrix ρ. This is instead of working directly with the subsystem Hamiltonian.

The principle of this method is a little more complicated than the previous cases. See the scheme on figure 3.8. We have a left block, right block and two sites in the middle, or $LqqR$, with dimensions $m_l \times q \times q \times m_r$. First we let both

blocks grow site by site, keeping m eigenstates of ρ with the largest eigenvalues (for explanation see chapter 4).

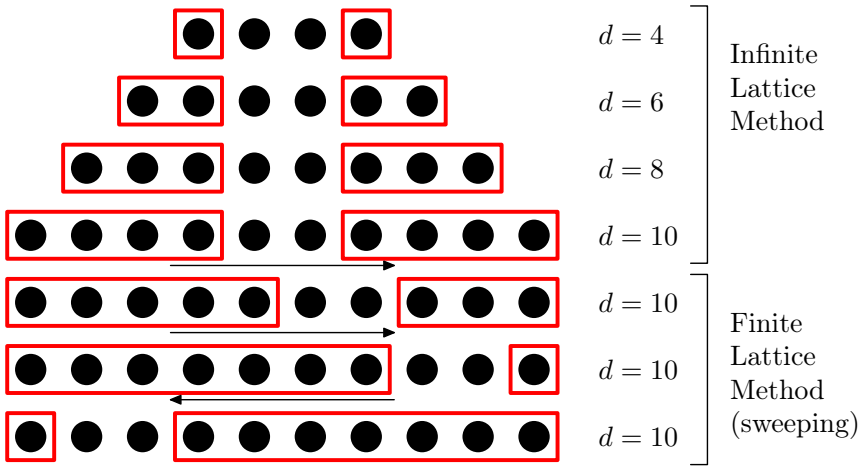

Figure 3.8: Scheme of forming the block in the Density Matrix Renormalization Group method. First the so called infinite-lattice method is employed to grow the block to desired size L and then the finite lattice method carries out the sweeping procedure. (from Szalay et al. [2015])

When they reach size L, we start assymetricaly enlarge left block at the expense of the right block. Right block now represents environment, whose interaction with left block we use to optimize its Hamiltonian iteration after iteration.

When the right block shrinks to the size of one lattice site, we start moving in the opposite direction and continue all the way to enlarge the right block to its maximal size $L-3$. This procedure is called *sweeping* and it leads to optimization of hamiltonian based on both the intrablock and interblock interactions. On top of that, from this algorithm, we can directly obtain the MPS form of the ground state (see chapter 4). But this holds to certain extent also for BRG and NRG. What makes the difference is really the way in which we truncate the subsapces and transform our quantum state and operator. The DMRG method respects the entanglement structure of the system. The amount of correlation can be measured by the number $m_{l,r}$ of left/right subspace states, which we need to keep in order to make the truncation error in reasonable bounds.

After few sweeps, the wavefunction and Hamiltonians are usually already approximated with a high precision, easily reaching the desired chemical accuracy.

In DMRG, we can estimate the truncation error and complexity of the method, and work in close contanct with the entanglement structure of the system. This makes it a method suitable for larger systems, chemical systems and strongly

correlated systems with nonlocal interactions. Unfortunately, for large systems, it is still impossible to simulte them, limiting us to work with still quite small molecules, with practical computational maximum of systems with around 64 sites.

But still, according to Schollwöck [2011], the DMRG is currently being recognized as the most powerful amongst the numerical methods for study of one-dimensional quantum lattices, and speaking more generally, one of the most efficient methods for simulating strongly correlated systems with linear (1D) entanglement pattern. The next chapter, chapter 4, is devoted solely to the description of the DMRG method and aims to bring light to its principles.

3.2.4 Tree Tensor Network States

As we have mentioned earlier in chapter 2, the *Tree Tensor Network State* is the generalization of the Matrix product state for higher dimensional lattice. These tensor product states have been designed to be compatible eith the DMRG method, since thay have the structure of a tree. A tree is a acyclic graph, that means it doesn't contain any circle in its structure. Therefore we can define order in whoch the DMRG is performed along the tree, visiting all of its branches, dividing the system into two large blocks and two small sites. This wouldn't be possible in a cyclic graph, since the two blocks could in general be connected and interact even on the *intrablock* level.

The algorithm for doing DMRG in the tree lattice (tensor network) is called the *Tree Tensor Network State algorithm* and for computations, it is an order of magnitude more demanding than the normal DMRG. It can be only run on the biggest supercomputers of our time. However, it has a potential of solving quantum chemical problems with strong 2D or 3D entanglement structure that used to be considered intractable on classical computers (see Nakatani and Chan [2013] for further reference).

4. Density Matrix Renormalization Group

In this chapter, we will introduce the algorithm of the renormalization group methods in detail, reflecting the historical development of methods leading to discovery of DMRG. Then we will explain the principle of DMRG and describe some related technicalities.

4.1 Real-space renormalization of Hamiltonians

Here we will formulate the numerical renormalization technique (RG) in terms of density matrices (DMRG) for arbitrary quantum lattice systems, as described in the original paper of White [1992]. For the sake of simplicity, we will explain the priciples on one-dimensional zero-temperature real space version of our model. In priciple, thanks to our density matrix approach, the above case can be later generalized to 2D or 3D case, or to momentum space (mostly loosing some scaling efficiency). This approach doesn't suffer from the common minus sign problem of the Monte Carlo methods and it is quite stable even for strong couplings and disordered systems.

For educational reasons, let us first describe the numerical renormalization method on 1D lattice of real-space blocks, forming together the full Hilbert space of the system in question. We will use the spin-$\frac{1}{2}$ Heisenberg model, as a typical example of a system that has such structure naturally, even though this blocking can be used for a general quantum system.

In infinite lattice RG method, we carry out a following procedure:

1. First we split the infinite lattice into equal blocks A.
2. Then we consider a subsystem AA of the two neighbouring blocks together and we diagonalize its Hamilonian H_{AA}.
3. Now we use m lowest-lying eigenstates of AA to form an approximate Hamiltonian $H_{A^{(2)}}$.
4. We repeat the procedure with larger blocks $A^{(i)}$ and their respective effective Hamiltonians $H_{A^{(i)}}$. See figure 4.1 for a schematic picture.

Obviously we assume here that the m lowest lying eigenstates are dominant and

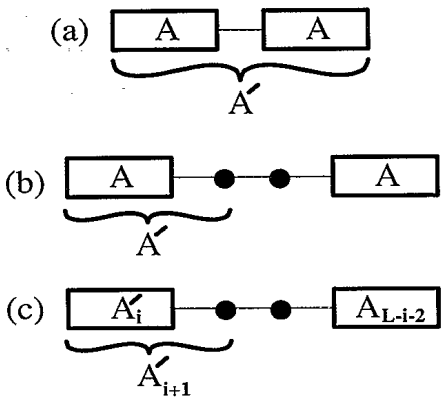

Figure 4.1: Various blocking schemes for one-dimensional renormalization group methods. (a) Standart approach for NRG. (b) Infinite lattice method. (c) Finite lattice method. in (b) and (c), we first diagonalize the entrire system and then form a reduced density matrix for the part labelled as A'. Lattice sites are depicted by the solid circles. (from White [1992])

play a leading role in forming the larger blocks. We will discuss this assumption in the further text.

Numerical RG provides a smart approximation and was the first effective solution to the Kondo problem, introduced in the paper of Wilson [1975]. Unfortunately, this approach is flawed with errors originating from the way it treats the boundaries of block. For most problems, such errors make it impossible to get quantitatively accurate results, as was shown by White and Noack [1992].

For forming the effective Hamiltonian of the larger block, we will use analogical approach as Wilson did for Kondo problem. This involves changing the basis to the set of m lowest lying eigenstates. Denoting the corresponding transformation matrices as O, this yields

$$H_{A^{(2)}} = O H_{AA} O^{\dagger}. \tag{4.1}$$

Here the dimesion of O is $m \times r$, with $r \coloneqq \dim H_{AA}$. As one may expect, the rows of O are the m lowest-lying eigenstates of H_{AA}. The procedure carried out above for the Hamiltonian operator is the so called renormalization present in the name of RG methods.

The above mentioned boundary errors originate from our selection of the lowest-lying energy eigenstates of AA and following subsystems. However our selection is natural, it neglects the influence of interaction of such blocks. H_{AA} has no connection with neighbouring blocks and thus its eigenstates will reflect this fact, leading to errors and non-physical behaviour at the block boundaries. In most systems, these blocks interact with each other and we need to modify our algorithm to take

this into account. In following chapter, we show how to choose the optimal set of the new basis states, allowing us to use the RG method even for interacting systems.

4.2 Density matrices and DMRG truncation

In order to select an optimal set of basis states for approximating the enlarged block system in RG methods, we present a Density Matrix Renormalization Group method, introduced in White [1992]. The basic idea can be outlined on the grounds of a superblock method proposed by White and Noack [1992].

Consider a superblock composed of three or more A blocks. Now think about which basis states should we choose to efficiently represent our subsystem AA. The idea is to consider the lowest energy eigenstates of the superblock and project those to our sybsystem AA in order to get our desired set of basis states of AA. However, the projection of superblock eigenstates to AA is not clearly defined for a many-particle wave function. Also in general, we have to consider a projection operation onto a complete set of block states. We need to find a way to select the most influential states in this projection. In the text to follow, we will show that the optimal strategy is to keep the eigenvectors with the largest eigenvalues of the density matrix of AA.

Let's assume that we know the state of the whole lattice, a pure state $|\psi\rangle$. Our task is to find m states that represent the lattice state most effectively, that is, to truncate the basis and keep only m states. More fashionable name for such procedure is "lossy quantum compression".

Remark. Assuming the pure state here is only for simplicity and the following conclusions would stay unchanged either for a mixed state or for a system at finite temperature. See White [1992] for further reference.

First we fix the basis as

$$|\psi\rangle = \sum_{i,j} \Psi_{ij} |i\rangle |j\rangle , \tag{4.2}$$

where $|i\rangle$, $i = 1 \dots r$ is the basis of AA and the states $|j\rangle$ indexed by j form basis of the rest of the lattice. Assume for simplicity that coefficients Ψ_{ij} are real. We are looking for m states $|u^\nu\rangle$, with $m < r$ approximating $|\psi\rangle$ like

$$|\psi\rangle \approx \sum_{\nu,j} c_{\nu j} |u^\nu\rangle |j\rangle , \tag{4.3}$$

where $c_{\nu j}$ is a real rectangular matrix. Now the reduced density matrix for AA is

$$\rho_{ii'} \equiv \sum_j \Psi_{ij} \Psi_{i'j}. \tag{4.4}$$

Notice the trace over j, the rest of the lattice. Now we can express the error of our lossy compression

$$\sigma = \left\| |\psi\rangle - \sum_{\nu,\, j} c_{\nu j} \, |u^{\nu}\rangle \, |j\rangle \right\|. \tag{4.5}$$

We will attemp to minimize the error σ with respect to $c_{\nu j}$ and $\langle i|u^{\nu}\rangle$. Looking for $|u^{\nu}\rangle$ orthogonal $\left\langle u^{\alpha}\middle|u^{\beta}\right\rangle = \delta^{\alpha\beta}$.

Theorem 1. *To minimize the error σ under above assumptions, the optimal solution states $|u^{\nu}\rangle$ for $\nu = 1 \ldots m$ are the eigenvectors of reduced density matrix ρ with the largest eigenvalues ω_{ν}.*

Proof. Let us use the norm definition $\||x\rangle\|^2 \equiv \langle x|x\rangle$ to express the error

$$\sigma^2 = \left(\langle\psi| - \sum_{\mu,\, j} c_{\mu j} \, \langle j| \, \langle u^{\mu}| \right) \left(|\psi\rangle - \sum_{\nu,\, l} c_{\nu l} \, |u^{\nu}\rangle \, |l\rangle \right) = \tag{4.6}$$

$$= \sum_{i,j,k,l} \Psi_{ij}\Psi_{kl} \, \langle i|k\rangle \, \langle j|l\rangle - 2 \sum_{i,j,\nu,l} \psi_{ij} c_{\nu l} \, \langle i|u^{\nu}\rangle \, \langle j|l\rangle + \tag{4.7}$$

$$+ \sum_{\mu,j,\nu,l} c_{\mu j} c_{\nu l} \, \langle u^{\mu}|u^{\nu}\rangle \, \langle j|l\rangle \, , \tag{4.8}$$

where $\langle j|l\rangle = \delta_{jl}$. So, thanks to the orthogonality, we can simplify to

$$\sigma^2 = \sum_{i,j} \Psi_{ij}\Psi_{ij} - 2 \sum_{i,j,\nu} \psi_{ij} c_{\nu j} \, \langle i|u^{\nu}\rangle + \tag{4.9}$$

$$+ \sum_{\nu,j} c_{\nu j} c_{\nu j}. \tag{4.10}$$

From the definition of eigenstate of operator $\hat{\rho}_{ii'}$ we obtain

$$\hat{\rho}_{ii'} \, |u^{\nu}\rangle = \sum_{j} \Psi_{ij}\Psi_{i'j} \, |i'\rangle \, \langle i|u^{\nu}\rangle = \omega_{\nu} \, |u^{\nu}\rangle \tag{4.11}$$

Now we can move to the eigenbasis of $\rho_{ii'}$, we'll call it $\left|\tilde{i}\right\rangle$. There the matrix $\rho_{ii'}$ is diagonal, with eigenvalues $\left(\tilde{\Psi}_{ii}\right)^2$. If we fix $|u^{\nu}\rangle$ to be the eigenstates, then we have $\left\langle \tilde{i}\middle|u^{\nu}\right\rangle = \delta_{i\nu}$ and things simplify considerably

$$\hat{\rho}_{ii'} \, |u^{\nu}\rangle = \sum_{j} \Psi_{ij}\Psi_{i'j} \, |u^{\nu}\rangle \, \delta_{i\nu} = \omega_{\nu} \, |u^{\nu}\rangle \, , \tag{4.12}$$

$$\omega_{\nu} = \sum_{j} \Psi_{ij}\Psi_{\nu j} \left\langle \tilde{i}\middle|u^{\nu}\right\rangle = \sum_{j} \Psi_{\nu j}\Psi_{\nu j}. \tag{4.13}$$

Here the term for eigenvalue ω_ν is similar to one of the error terms. That can inspire us to set $c_{\nu j} \coloneqq \Psi_{\nu j}$. Putting all together, we are left with

$$\sigma^2 = \sum_j \left[\sum_i \Psi_{ij}\Psi_{ij} - \sum_{\nu i} \underbrace{\Psi_{\nu j}\Psi_{\nu j}}_{\omega_\nu} \delta_{\nu i} \right] . \tag{4.14}$$

This implies that our choice of selecting eigenvectors $|u^\nu\rangle$ with the largest eigenvalues ω_ν is justified and our statement is proven. □

Remark. Density matrix eigenvalues ω_ν express the probability to find the system AA in its eigenstate $|u^\nu\rangle$. The sum of eigenvalues, $P_m = \sum_\nu \omega_\nu$ tells us the probability of AA to be within the considered approximated set of states, and so $1 - P_m$ measures the accuracy of the truncation to m states.

4.3 Infinite and Finite-system DMRG

So when we have the eigenstates, we know how to pick the relevant ones. But let's discuss a bit more the diagonalization itself. Say we have a lattice of p identical blocks and we want to diagonalize the Hamiltonian. This approach, used in the article of White and Noack [1992], is ineffective for many-body problems, since the Hamiltonian dimension grows as m^p, having m states per block.

In contrast, one particulary efficient configuration is described in the famous paper by White [1992]. There the superblock is formed from two big blocks and two smaller lattice sites. We will use a notation LqqR for such configuration, which you can see on figure 4.2. Now L is the big block on the left, R is the right block and q, q are the two sites in the middle. Each of the big blocks corresponds to A above, with dimension m. In such configuration, the Hilbert space dimension is $O(m^2)$. In each iteration, we will add the neighbouring site to block L and R.

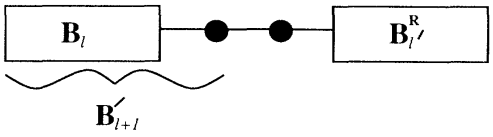

Figure 4.2: The LqqR configuration used for the DMGR calculations. Left rectangle represents the block L, then there are two sites q,q in the middle and the right block R. (from White [1993])

Let us sketch one iteration of the Density Matrix Renormalization Group algorithm for infinite lattice as presented in White [1993].

1. Make four initial blocks LqqR, each consisting of a single site at the beginnning, representing the four site system to stat with.

2. Form Hamiltonian in sparse matrix form for the superblock.

3. Using the sparse matrix Davidson or Lanczos algorithm, diagonalize the Hamiltonian of system LqqR in order to find the target state, usually the ground state.

4. Apply the equation 4.3 to express the reduced density matrix ρ of the two extended blocks Lq and qR.

5. Diagonalize ρ to obtain m of its largest eigenvalues ω_ν and their respective eigenvectors $|u^\nu\rangle$.

6. Form the relevant operators for each of the four blocks LqqR.

7. Transform to the new truncated basis using the equation 4.2, with vectors $|u^\nu\rangle$ as rows of the transformation matrices O. Transform block and all the relevant operators using the equation **?**.

8. For the following iteration, take the current extended block Lq as the new L and instead of old R use the reflection of new block L.

9. Go to step 2.

Remark. The method used for truncating the block L and R basis to m states is designed specifically to find one target state of the system LqqR. Not multiple, e.g. the excited states of LqqR. However, the above method can be modified to calculate multiple states. For more information on calculating the excited states, see Chandross and Hicks [1999].

Now we will cite the algorithm for finite-lattice method as described by White [1993]. The finite-lattice method works with a fixed superblock size L, iterating from left to right and back to optimize the block representations.

Both the infinite and finite-lattice methods are used in the DMRG. First the infinite method is used to grow the superblock to the target size L and then the finite lattice method improves the block representation and the related wavefunction by sweeping (sweep means that the algorithm passe the whole lattice, site by site). This procedure iteratively converges to the ground state of the system. We will describe the finite lattice method already including the intialization by the infinite-lattice method. We will denote the number of current iteration by i. Each iteration consists of $L-3$ steps indexed by the left block size l.

1. (First half of i) Use the infinite-lattice method to build the lattice to L sites. At each iteration store the block Hamiltonian and end operator matrices for the left block. Label blocks as B_l by their size $l = 1..L/2$.

2. (Start of the second half of $I = 1$) Set $l = L/2$. Use B_l as left block and the reflection of B_{L-l-2} as the new right block.

3. Do steps 2.-8. of the infinite lattice method.

4. Store the new left block as B_{l+1}, replacing the old block.

5. Replace the right block with a reflection of B_{L-l-2}, obtained from the first half of this iteration.

6. If $l < L - 3$, set $l = l + 1$ and go to step 3.

7. (Start of iteration i for $i > 2$) Make four intial blocks, the first three with just a single site a the right block consisting of the reflection of B_{L-3} from previous iteration. Set $l = 1$.

8. Follow steps 2.-8. from the infinite-lattice method.

9. Store the new left block as B_{l+1}, replacing the old block.

10. Replace th right block with a reflection of B_{L-l-2}, obtained from the previous iteration (if $l \leq L/2 - 1$) or the first half of this iteration ($l > L/2 - 1$).

11. If $l < L - 3$, set $l = l + 1$ and go to step 8. Else if $l = L - 3$, start a new iteration by going to step 7. (Stop after 2 or 3 iterations.)

For simplicity we assumed even L. After few iterations, each B_l accurately represents an l-block, which is the left l sites of an L-site chain. This method reaches good accuracy or even converges already in the middle of the second sweep. Usually two or three sweeps are sufficient.

When the finite-lattice DMRG converges we have the ground state of the Hamiltonian and we can also have all the required operators renormalized in the subsequent steps, if we keep track of them, or we can just keep track of the O matrices from the equation 4.1 and carry out the renormalization after the DMRG, when required for any arbitraty operator. The arbitrary operator X then has the form of

$$X = O_{L-1}...O_2O_1\, X_1\, O_1^\dagger O_2^\dagger ... O_{L-1}^\dagger, \tag{4.15}$$

where the lower index corresponds the number of sites for the block for which we form the operator X in each subsequent iteration step.

Remark. Note that there is a very important correspondence between the DMRG procedure and the MPS formalism. It is possible to reindex the transformation matrices O from the equation 4.1 generated in each step of DMRG to obtain the A matrices of the MPS formalism. Thus we are able to get the MPS decomposition from a DMRG sweep.

4.4 Entanglement-based Optimizations for the DMRG method

4.4.1 Schmidt Ranks and the dynamic block state selection

Even though the simplest approach is to truncate the blocks at each iteration to some fixed size of m states, we can also adapt the block size dynamically in such way that the quantum correlations are preserved as much as possible. According to Legeza et al. [2003], such approach is more efficient in terms of our control of the truncation error δ_ϵ, making δ_ϵ more stable to fluctuations during the DMRG sweep (see figure 4.3). This procedure is called the *dynamic block state selection* (DBSS) and it's based on a gradual enlargement of the block sizes, such that the estimate of the truncation error is kept bellow a user defined maximum.

Another important quantity we need to keep track of is the quantum information loss. When we enlarge a block of size l by one site and truncate, the entropy of the resulting block $S^{(l+1)}$ is lower than the sum of entropies $S^{(l)}$ and $S^{(1)}$ of the former subsystems

$$S^{(l)} + S^{(1)} - S^{(l+1)} = I_l \geq 0, \tag{4.16}$$

where I_l is the mutual information describing the correlation between the former block and the newly added orbital. In case $I_l > 0$, we have to consider increasing the number of states kept for the new block, since we need more information to describe the enlarged block.

The total information gain during one sweep is $\sum_i = 1^L I_i$. In general case I_i is a function of subsequent sweeps. But according to Szalay et al. [2015], from the moment when the DMRG converges on, the $S^{(l)}$ and $S^{(1)}$ don't change any more.

The fancy-named DBSS is in fact a very simple procedure which after each enlargement of block with m states increases the number of block states $m' \leq m \times q$ until the following condition is satisfied

$$S^{(l)} + S^{(1)} - S^{(l+1)}_{\text{truncated}} < \chi, \tag{4.17}$$

where χ is the predefined boundary for the error induced by the correlation loss.

With DBSS, we can guarantee that the entanglement between the blocks doesn't get truncated dramatically and we can predefine a desired accuracy.

Remark. The risk of converging into a local minima leads to a neccessity to introduce the minimum number of block states $m_{\min}$. According to Szalay et al. [2015], the practical experience is that $m_{\min} = q^3$ or q^4 is usually sufficient. In order to limit the computational complexity of the simulation, we need also to set an upper boundary $m_{\max}$.

4.4.2 Optimizing the basis

Working in the right basis set is among the most important properties in terms of optimization of any simulation or physical theory. The most common cost function for optimizing the basis in quantum chemistry is the energy. Observing its convergence provides us with information essential for monitoring the quality of our choice. However, it's not the only quantity to look for in this context.

Quantum Information Theory offers us tools for analysis of the entanglement structure. As we have emphasized in section 3.1.1, in many cases its structure has to be taken into account for quantum-chemical or solid-state physics problems. This holds also for basis optimization.

When we select an appropriate basis, we should analyze the quantum correlations between and inside the orbitals of our system and select the basis that respects this entanglement pattern. Our choice is then reflected in mutual information, overall entanglement and other quantities measuring entanglement, which are usually strongly basis dependent. The choice of basis has also a major influence on the convergence properties and performance of DMRG. For instance, with the appropriate set of basis states, representing equal quantum state may require significantly smaller amount of block states (see Wouters et al. [2014]).

The main objective is to find such basis, in which the entanglement is localized inside the orbitals. In such setup, a smaller number of states is necessary to represent the block with desired accuracy.

Let me cite an example of basis optimization for DMRG method by Murg et al. [2010]. This group optimized basis via the canonical transformation of the fermionic modes, using a $q \times q$ unitary matrix U. The cost functoin was the energy E, whose calculation was implemented via the following formula based on the Hamiltonian. They applied a gradient search to the function

$$E\left(U\right) = \sum_{ij} \left(UTU^{\dagger}\right)_{ij} \langle a_i^{\dagger} a_j \rangle + \sum_{ijkl} \left[\left(U \otimes U\right) V \left(U \otimes U\right)^{\dagger}\right]_{ijkl} \langle a_i^{\dagger} a_j^{\dagger} a_k a_l \rangle, \quad (4.18)$$

where T and V are the single electron and two electron integrals corresponding to the kinetic and potential part of Hamiltonian respectively. Here $a_i^{\dagger}$ and a_i are the fermionic creation and annihilation operators (for quantum chemistry). Expectetaion values $\langle a_i^{\dagger} a_j \rangle$ and $\langle a_i^{\dagger} a_j^{\dagger} a_k a_l \rangle$. Can be calculated separately with

respect to the original state, since they're independent on U. The gradient of $E(U)$ can be calculated explicitely and quite efficiently, allowing for repeated calculation during the network optimization.

4.4.3 Optimizing the MPS initialization

The initial performance of SVD is strongly influenced by the initial matrix configurations in our MPS state. Wrong choice of inital approximation may lead our DMRG calculation to the local minima (see Moritz and Reiher [2006]).

In the first iteration, the values of the matrix elements are usually initialized as random numbers. When we perform SVD to select most relevant states in the left block, the result eigenstates of the density matrix ρ are higly dependent on the basis states used to construct the right (environment) block. In the real quantum system, the state of the subsystem tends to be strongly entangled with the enviroment. Thus, in order to recreate the realistic initial conditions, we need to find such representation of the environment block, which maximizes the von Neumann entropy $S^{(l)}$ of the left block (see Szalay et al. [2015]).

This can be achieved by selecting the orbitals with the higest single-orbital entropy values. The vector of orbitals sorted by one-oribital entropy is called the CAS-vector. It can be determined based on the chemical considerations about the system, or it can be obtained directly from the entropy calculation.

This optimization has been extendent by exploiting features of the familiar *Configuration Interaction* (CI) procedure. Here the wave function is writen in terms of a linear combination of determinants with expansion coefficients given by the requirement of minimizing the energy. The determinants labelled as s, d, t correspond to the singly, doubly, triply, etc. excited relative to the Hartree-Fock (HF) configuration. The CI wave function can be written as

$$\Psi = c_{HF}\Phi_{HF} + \sum_s c_s\Phi_s + \sum_d c_d\Phi_d + \sum_t c_t\Phi_t + ... \tag{4.19}$$

The number of determinants is increased systematically in order to achieve higher accuracy.

When the HF wavefunction is known, we can keep only the states of the right block which together with the state of the left block describe some of the excited states corresponding to a given CI-level, with respect to the HF. Then the right block contains state for a given CI-level and the total wave function can contain higher excitations thanks to the correlations between the blocks. This alows us to control the minimum CI-level and together with the CAS ordering in each iteration, the double optimization is carried out. This yields a useful interconnection between the enviroment block states, which are in each step constructed based on the

renormalized left block states and the left block states which are optimized during the SVD to best fit the well represented environment block. Then the the reduced density matrix of the left block is well defined and we can use DBSS (see section 4.4.1) to truncate it appropriately.

This so called CI-DEAS procedure guanrantees a presence of several strongly entangled orbitals from the very beginning. Both static and dynamic correlations are taken into account and the risk of falling into local minima is minimized. This procedure efficiently finds most of the correlation energy and after the initialization is over, that is after half a sweep, the chemical accuracy is reached (see Szalay et al. [2015]).

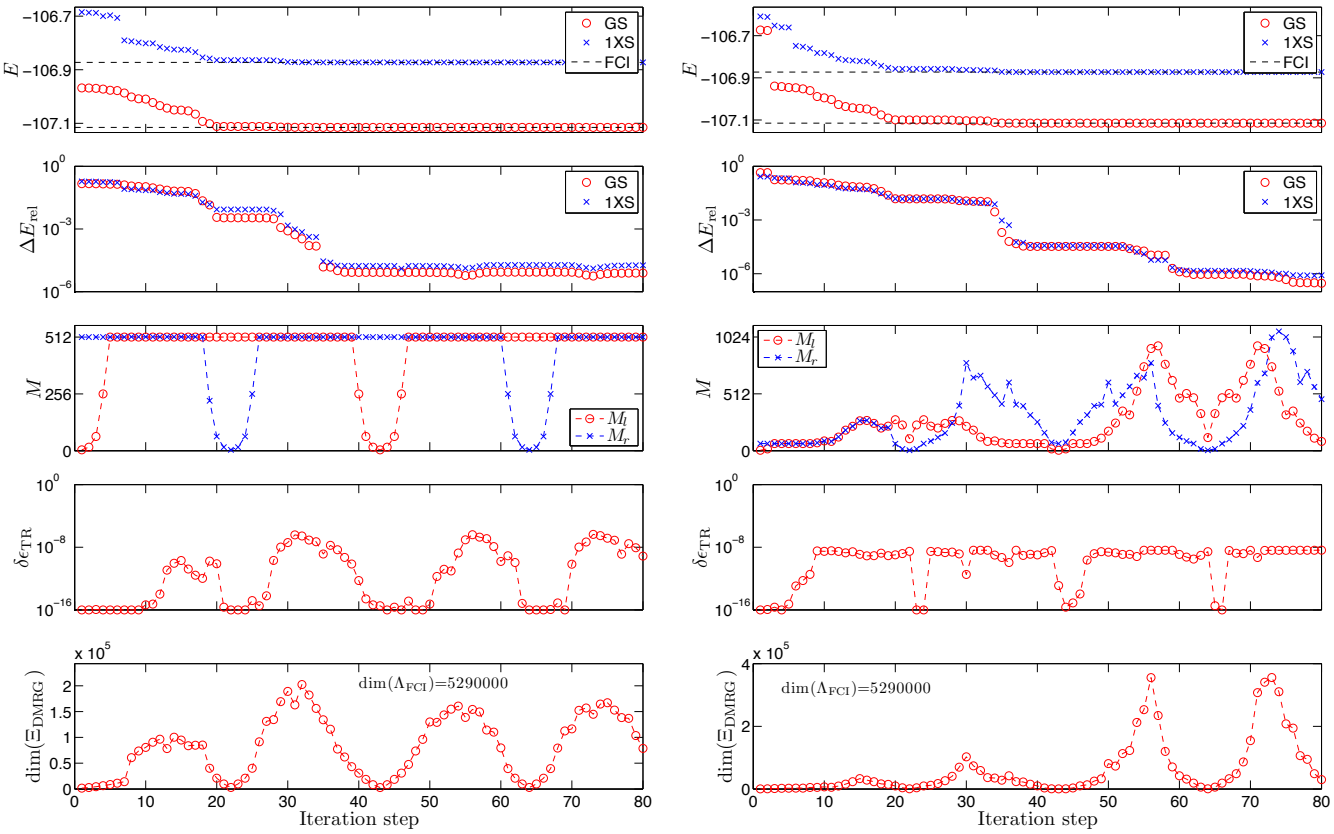

Figure 4.3: Plot of complex statistics of a DMRG sweep when simulating LiF molecule at bond length $d = 3.05$ a.u. for fixed number of block states. We can see the energy E of the ground state in atomic units, relative error $(E_{\mathrm{DMRG}} - E_{\mathrm{FCI}})/E_{\mathrm{FCI}}$ for comparing the DMRG energy with precise Full Configuration Interaction method, number of block states M_l, M_r, truncation error $\delta_{\epsilon_{\mathrm{TR}}}$ and the dimension Ξ_{DMRG} of the superblock as a function of DMRG iteration steps. On the left side, there are graphs for non-optimized ordering and on the right the tensor hiearchy (ordering) was optimized prior to the simulation. (from Szalay et al. [2015])

5. Practical Part: Multipartite Entanglement Patterns and Correlations

The main aim of this master thesis was to design a module for the universal Budapest DMRG code for calculating three-site reduced density matrix, mutual information and correlations of general operators acting on three sites. Budapest DMRG is a complex system for simulating quantum mechanical models from solid state physics and quantum chemistry. It is written in MATLAB and compiled in C and some of its part are prepared for parralel computations. Even our module had to be parallelized to be able to run on computer clusters with multiple machines and multiple processor cores, designed for large scale computations.

After finishing the development and verifying correctness of the program with several exact simulations, we have carried out a demonstrational simulation of the diborane molecule, a well known example of a molecule with unusual bonding, namely with 3-orbital 2-electron bonds. The goal of our demonstration was to determine whether bonds in diborane exhibit the three-site correlations.

The module was included in the production version of Budapest DMRG and will be used by our group and by the Budapest-based group for practical calculations of chemically interesting systems with intention to study the multipartite correlations and investigate the entanglement patterns of these systems.

In this chapter, we are going to describe our solution and practical calculations.

5.1 Generalized Correlation Functions

In this section, we are going to describe how the mutual information was calculated using the *generalized correlation functins* introduced in chapter 3.1.4. This section aims to present the relevant terms from the viewpoint of practical calculations.

First let's clarify the system partition we work at. When the reduced density matrices ρ_{ij}, ρ_{ijk} are calculated, the system is effectively split into three, respectively four subsystems. Thus a generalization of the usual definition of bipartite entanglement must be taken into account. For tripartite systems or systems with

four partitions, the wavefunction is decomposed as

$$|\Psi\rangle = \sum_{u_i\, u_j\, \beta} c_{u_i u_j \beta}\, |u_i\, u_j\, \beta\rangle\,,$$
$$|\Psi\rangle = \sum_{u_i\, u_j\, u_k\, \beta} c_{u_i u_j u_k \beta}\, |u_i\, u_j\, u_k\, \beta\rangle\,, \tag{5.1}$$

where we used our usual notation for labelling the bases of lattice sites i, j and k with u_i, u_j and u_k. For the rest of the system (the environment), we used index β. For the tripartite system, that is, for calculating the two-site reduced density matrix, the generalized correlation function can be expressed as

$$\begin{aligned}\langle\Psi|\, T^{(u'_m\, u'_n)}_{(u_m\, u_n)}\, |\Psi\rangle &= \sum_{u'_i\, u'_j\, \beta'} \sum_{u_i\, u_j\, \beta} c^{\star}_{u'_i u'_j \beta'}\; c_{u_i u_j \beta}\, \left\langle u'_i\, u'_j\, \beta' \right|\, T^{(u'_m\, u'_n)}_{(u_m\, u_n)}\, |u_i\, u_j\, \beta\rangle\,,\\ &= \sum_{\beta,\,\beta'} c^{\star}_{u'_m u'_n \beta'}\; c_{u_m u_n \beta}\, \langle u'_m\, u'_n\, \beta' | u_m\, u_n\, \beta\rangle\,,\\ &= \sum_{\beta} c^{\star}_{u'_m u'_n \beta}\; c_{u_m u_n \beta} \equiv (\rho_{mn})_{u'_m\, u'_n\, u_m\, u_n}\,,\end{aligned} \tag{5.2}$$

where in the last step, we assume that we work in the orthonormal basis.

The generalized correlation function measures the amplitude of the transition between initial and final state with respect to the environment. Therefore it depends on the amplitude of the coefficients of the two states.

For example, the reader might imagine the singlet valence bond between orbitals witch spin-$\frac{1}{2}$ degrees of freedom. For such example, we may use $\langle T^{(u'_m\, u'_n)}_{(u_m\, u_n)}\rangle$ directly for characterizing the bond.

In general, the value of $\langle T^{(u'_i\, u'_j)}_{(u_i\, u_j)}\rangle$ might scale to a finite value with respect to the distance of the sites i, j on the lattice. According to Barcza et al. [2015], this scaling may occur even for many-body states without a long-range order. In such case, we can choose to study the *connected part of the generalized correlation function*

$$\langle T^{(u'_i\, u'_j)}_{(u_i\, u_j)}\rangle_{\mathrm{C}} \equiv \langle T^{(u'_i\, u'_j)}_{(u_i\, u_j)}\rangle - \langle T^{u'_i}_{u_i}\rangle \langle T^{u'_j}_{u_j}\rangle, \tag{5.3}$$

where we subtract the possibly disconnected part fully contained in $\langle T^{u'_i}_{u_i}\rangle \langle T^{u'_j}_{u_j}\rangle$. Note that the mutual information is defined in equation (3.5) in the similar manner, that the disconnected part doesn't contribute.

For a better picture, we will show a practical example of building two-site reduced density matrix from the generalized correlation functions. We will consider a simple model of L spin-$\frac{1}{2}$ particles on the one-dimensional lattice. We will label the spin-up and spin-down basis states with $|\uparrow\rangle$ and $|\downarrow\rangle$.

Since the dimesion of one lattice site is $q = 2$, there are $q^2 = 4$ transition operators $\langle T^{u'_i}_{u_i} \rangle$ with $u, u' = \uparrow, \downarrow$ and $i = 1..L$. Then for example the transition $|\uparrow\rangle_i \longmapsto |\downarrow\rangle_i$ on site i will be carried out by the operator $T^{\downarrow_i}_{\uparrow_i}$ and the transition $|\downarrow_i\uparrow_j\rangle \longmapsto |\uparrow_i\downarrow_j\rangle$ on sites i, j by the operator $T^{\downarrow_i\uparrow_j}_{\uparrow_i\downarrow_j}$. We will use shorthand notation $T^{\downarrow\uparrow}_{\uparrow\downarrow}$ when its obvious which sites are involved in the transition. Analogously, we will use the three-site transition operators $T^{(u'_i\, u'_j\, u'_k)}_{(u_i\, u_j, u_k)}$ introduced in equation (3.17).

Now we will discuss forming of the reduced density matrix, beginning with the two-site version ρ_{ij}, since the calculation of the one-site case has already been described in chapter 3.1.4. First we should emphasize that the reduce density matrix is usually a sparse matrix and to optimize it's calculation, we should focus only on the nonzero elements. First note that from its definition, the reduced density matrix preserves certain quantum numbers, like in this case the overall spin. Thanks to this symmetry, we know that we don't have to calculate the matrix elements corresponding to the transitions which change the total spin. The nonzero matrix elements, are listed in the table 5.1. We see that we need to calculate only the expectation values for the listed operators, which is 6 out of 16 matrix elements. For higher dimensional site $SU(n)$ model, this optimization becomes significant and for the three-site reduced density matrix, it is particularly important, since the total number of matrix elements scales like $q^3 \times q^3$.

ρ_{ij}	$\|\downarrow\downarrow\rangle$	$\|\downarrow\uparrow\rangle$	$\|\uparrow\downarrow\rangle$	$\|\uparrow\uparrow\rangle$
$\|\downarrow\downarrow\rangle$	$\langle T^{\downarrow\downarrow}_{\downarrow\downarrow} \rangle$			
$\|\downarrow\uparrow\rangle$		$\langle T^{\downarrow\uparrow}_{\downarrow\uparrow} \rangle$	$\langle T^{\uparrow\downarrow}_{\downarrow\uparrow} \rangle$	
$\|\uparrow\downarrow\rangle$		$\langle T^{\downarrow\uparrow}_{\uparrow\downarrow} \rangle$	$\langle T^{\uparrow\downarrow}_{\uparrow\downarrow} \rangle$	
$\|\uparrow\uparrow\rangle$				$\langle T^{\uparrow\uparrow}_{\uparrow\uparrow} \rangle$

Table 5.1: Nonzero elements of the two-site reduced density matrix for one-dimensional spin-$\frac{1}{2}$ lattice. Initial states are in the leftmost column, whereas final states are located in the top row.

Now let's move to the three-site case, still considering the example of one-dimensional spin-$\frac{1}{2}$ lattice. For the three-site reduced density matrix ρ_{ijk}, the number of nonzero elements is 36 out of 64 (see Szilvási et al. [2015]). You can see its block-diagonal stucture in table 5.2. Each block corresponds to a single value of the total spin. Note that the degeneracy subspaces are of different size compared with the two-site case in table 5.1.

ρ_{ijk}	$\vert\downarrow\downarrow\downarrow\rangle$	$\vert\downarrow\downarrow\uparrow\rangle$	$\vert\downarrow\uparrow\downarrow\rangle$	$\vert\uparrow\downarrow\downarrow\rangle$	$\vert\downarrow\uparrow\uparrow\rangle$	$\vert\uparrow\downarrow\uparrow\rangle$	$\vert\uparrow\uparrow\downarrow\rangle$	$\vert\uparrow\uparrow\uparrow\rangle$
$\vert\downarrow\downarrow\downarrow\rangle$	$\langle T^{\downarrow\downarrow\downarrow}_{\downarrow\downarrow\downarrow}\rangle$							
$\vert\downarrow\downarrow\uparrow\rangle$		$\langle T^{\downarrow\downarrow\uparrow}_{\downarrow\downarrow\uparrow}\rangle$	$\langle T^{\downarrow\uparrow\downarrow}_{\downarrow\downarrow\uparrow}\rangle$	$\langle T^{\uparrow\downarrow\downarrow}_{\downarrow\downarrow\uparrow}\rangle$				
$\vert\downarrow\uparrow\downarrow\rangle$		$\langle T^{\downarrow\downarrow\uparrow}_{\downarrow\uparrow\downarrow}\rangle$	$\langle T^{\downarrow\uparrow\downarrow}_{\downarrow\uparrow\downarrow}\rangle$	$\langle T^{\uparrow\downarrow\downarrow}_{\downarrow\uparrow\downarrow}\rangle$				
$\vert\uparrow\downarrow\downarrow\rangle$		$\langle T^{\downarrow\downarrow\uparrow}_{\uparrow\downarrow\downarrow}\rangle$	$\langle T^{\downarrow\uparrow\downarrow}_{\uparrow\downarrow\downarrow}\rangle$	$\langle T^{\uparrow\downarrow\downarrow}_{\uparrow\downarrow\downarrow}\rangle$				
$\vert\downarrow\uparrow\uparrow\rangle$					$\langle T^{\downarrow\uparrow\uparrow}_{\downarrow\uparrow\uparrow}\rangle$	$\langle T^{\uparrow\downarrow\uparrow}_{\downarrow\uparrow\uparrow}\rangle$	$\langle T^{\uparrow\uparrow\downarrow}_{\downarrow\uparrow\uparrow}\rangle$	
$\vert\uparrow\downarrow\uparrow\rangle$					$\langle T^{\downarrow\uparrow\uparrow}_{\uparrow\downarrow\uparrow}\rangle$	$\langle T^{\uparrow\downarrow\uparrow}_{\uparrow\downarrow\uparrow}\rangle$	$\langle T^{\uparrow\uparrow\downarrow}_{\uparrow\downarrow\uparrow}\rangle$	
$\vert\uparrow\uparrow\downarrow\rangle$					$\langle T^{\downarrow\uparrow\uparrow}_{\uparrow\uparrow\downarrow}\rangle$	$\langle T^{\uparrow\downarrow\uparrow}_{\uparrow\uparrow\downarrow}\rangle$	$\langle T^{\uparrow\uparrow\downarrow}_{\uparrow\uparrow\downarrow}\rangle$	
$\vert\uparrow\uparrow\uparrow\rangle$								$\langle T^{\uparrow\uparrow\uparrow}_{\uparrow\uparrow\uparrow}\rangle$

Table 5.2: Nonzero elements of the three-site reduced density matrix for one-dimensional spin-$\frac{1}{2}$ lattice. Leftmost column contains the intial states, whereas final states are located in the top row. The block diagonal structure corresponds to the total spin conservation.

When we obtain ρ_{ij} and ρ_{ijk} in the block-diangonal form, it's straightforward to diagonalize it block by block and calculate the von Neumann entropy, for both the two-site case S_{ij} and three-site case S_{ijk}. For that we use equations 1.10 and 1.11. Then we can apply equations (3.5) and (3.6) to get the two-site and three-site mutual information I_{ij} and I_{ijk}. Of course for the one-site case it's even simpler, making use of the equations (1.9) and (3.4).

Let us emophasize once more that our calculations and whole the entanglement structure is basis dependent. We follow closely the method of Szilvási et al. [2015] to find a link between the chemical bonds and the mutual information.

5.2 Our Solution

Budapest DMRG code implements the classical version of DMRG, where the O matrices correspond with the MPS decomposition (see section 4.3), but the program still works with states in the traditional form of renormalization picture, without directly using MPS. In case of applications requiring the MPS formalism there is an option to use the post-DMRG analysis, which means that after the DMRG finishes, we convert the state to MPS form and work with it further. Our code doesn't use MPS directly and it can be used as a benchmark to compare with for MPS based three-site reduced density matrix calculations, thanks to it's general design and numerical performance.

In order to implement the procedure from the previous section for calculating the generalized correlation functions and the respective quantities, we had to make a program for efficient generating of the three-site operators based on equation 4.15. Then, having the operators $T^{(u'_i\, u'_j\, u'_k)}_{(u_i\, u_j, u_k)}$ in a sparse matrix form, respecting the symmetries of quantum numbers and having all the required O matrices in a compact form on the disk, we made a program for an effective contraction of the matrix form of $T^{(u'_i\, u'_j\, u'_k)}_{(u_i\, u_j, u_k)}$ with the wave function vector $|\Psi\rangle$. The script is able to calculate the expectation values required to obtain the generalized correlation functions and other three-site operators correlations using the powerful tensor product libraries from Budapest DMRG.

Our program for three-site operator correlations works in a following way

1. Load the definitions of single-site operators from which we build the three-site operators. Load the O matrices and other stored files generated by DMRG for basis tranformations and truncation. Load information about the actual model and intialize superblock.

2. Performing the enlarging of the block in the infinite-lattice procedure, renormalize operators with O matrices based on the Hamiltonian structure, quantum number denegeracy subspaces and phase factors. When the block size reaches the desired size (half of the lattice, see figure 3.8), the operators in the sparse form are ready for further use.

3. Store the sparse operators for each site combinations in form of a large vector of matrices. Using the fermionic/bosonic operators symmetry we store only operators for sites $i \leq j \leq k$. With our scripts and libraries from Budapest DMRG, the operators stored in this form may be multiplied, contracted with states and used like if they were in the full form. In case of need, we may reconstruct the full form.

4. Using our own script, contract the operator with wavefunction to obtain the expectation values. Thanks to respecting the symmetries of the system, tracking changes of quantum numbers and having our operators stored in a form compatible with the Hamiltonian structure, we may use the tensor libraries from Budapest DMRG to calculate the expectation value.

5.3 About the Implementation

When calculating the three-site reduced density matrix, first we have to find out which matrix elements are nonzero. To do this, we made another script which

automatically explores the basis states of subspaces where the two-site and three-site operators act. Then we are able to determine which combinations of transition operators $T^{u_i'}_{u_i}$ conserve the quantum numbers and thus correspond with nonzero matrix ements of ρ.

Another script we made takes care of building the block diagonal form of three-site reduced density matrix ρ_{ijk} introduced in the previous section. It builds ρ_{ijk} from the computed expectation values $\langle T^{(u_i' u_j' u_k')}_{(u_i u_j, u_k)} \rangle$, respecting the phase signs of general operator combinations and swapping positions on the lattice during the procedure (nontrivial technicality). Then the script reverts the optimized lattice ordering to the former form, diagonalizes blocks of ρ_{ijk} and from its eigenvalues ω_ν it calculates entropy and mutual information.

After calculating all the relevant quantities, we need to make sure that the values are correct. This is done (only for small systems, since the complexity scaling is exponential) using our script for exact calculation of the correlation functions. This script loads the single site operators and generates full form of these operators. It retains the full operator matrices in the memory, being very simple, however also very ineffective. It builds the full Hamiltionian and diagonalizes it to find the ground state wave funciton. Then it multiplies these matrices to build a three-site operator and calculates their correlations, contracting them with the ground state vector in order to calculate the expectation values. When building the full form of Hamiltonian and calculating its eigenvalues and eigenstates, the script uses a bruteforce MATLAB diagonalization. All the calculated quantities then proceed to an automated comparation script, which determines up to which accuracy were our calculations precise.

The last script I will describe handles the parallelization of the calculation of the generalized correlation functions. Since the number of nonzero matrix elements of three-site reduced density matrix may scale to hundreds of thousands for practical calculations, we need to be able to run them on a large computatinal cluster. For this we made a script that distributes the calculation to all available machines and processor cores. Thanks to the fact that each expectation value may be calculated independently, a simple bash script can just split the task in as many parts as many computers are available and distribute them accordingly. Then a second script parallelizes the calculation on a single machine via MATLAB parallel environment, to use all the free processor cores.

5.4 Summary of Used Approximations and Optimization Tricks

During our practical calculations, we have directly made use of following approximations, methods and optimization procedures, most of which are described in this thesis. We include also relevant links for further reference.

- Singular value decomposition. Section 2
- Density matrix Renormalization Group method and its advanced truncation. Chapter 4
- Dynamic block state selection using the entanglement structure. Please refer to section 4.4.1.
- Optimizing the initialization using the CI-DEAS procedure. Section 4.4.1.
- Ordering optimization using the Fiedler vector. See Szalay et al. [2015].
- Schmidt ranks optimization. Section 4.4.1.
- Quantum numbers symmetries. See Szalay et al. [2015].
- Sparse matrix storage optimization. See Eijkhout [1992].
- Davidson algorithm for diagonalization. See Crouzeix et al. [1994].
- Parallelizaton on bash level and using MATLAB parfor. See Sharma and Martin [2009] or the official documentation The MathWorks, Inc. [2016b].
- Effective pre-summation of Hamiltonian terms. See Szalay et al. [2015].
- Budapest DMRG tensor product libraries. See Szalay et al. [2015].
- MATLAB mcc compilation of MATLAB code to C. See official documentation The MathWorks, Inc. [2016a].
- Budapest DMRG feature of transforming all objects and classes to structures prior to compilation.

5.5 Diborane

5.5.1 Expected Behavior of Mutual Information

As a first demonstration of our module for three-site correlations, we calculated the entanglement pattern of diborane B_2H_6, whose structure can be seen in figure 5.1. This molecule exhibits three-site correlations related to its 3-centered 2-electron bonds on the B_2H_2 ring.

Based both on the chemical intuition and rigorous description from paper Laszlo [2000], we will now briefly sum up our expectations considering the behaviour of mutual information in diborane. We expect that the two site mutual information will reflect all the bonds visible on figure 5.1. However, it should not be present between the boron core orbitals 6, 12 and other orbitals (see the indexing in figure 5.2), since we don't expect the core orbitals to interact with other atoms.

There should be a correlation between boron and its outer hydrogens (not in the ring), as these are covalently bonded. But these hydrogens shouldn't be strongly correlated with other atoms.

Finally, for the three-mutual correlations, we expect them to take part in the 3-center 2-electron bonds in the ring. It can be either B-H-B, or H-B-H. Especially the orbitals heading in the direction along the ring should be responsible for these bonds.

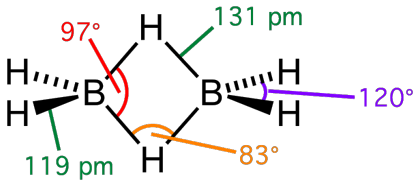

Figure 5.1: Stereo skeletal formula of diborane with all explicit hydrogens and assorted measurements. (from Wikimedia Commons [2016])

5.5.2 Results

The geometry of diborane was optimized at the DFT(B3LYP)/cc-pVDZ level. We followed the work of Szilvási et al. [2015] and Szalay et al. [2016] and studied the chemical bonding in terms of correlations of localized (atomic-like) orbitals. The canonical Hartree-Fock molecular orbitals were therefore localized by the Pipek-Mezey procedure with tight threshold 10-12 and minimized the number of atomic orbitals contributed in each localized orbitals. All preliminary calculations have been done by MOLPRO Version 2010.151 (see Werner et al. [2010]).

Using the procedure described above, we have calculated all the relevant nonzero combinations of transition operator expectation values, from which we formed the one-site, two-site and three-site reduced density matrices ρ_i, ρ_{ij} and ρ_{ijk}. Then we calculated one-site, two-site and three-site entropy S_i, S_{ij}, S_{ijk} and mutual information I_{ij} and I_{ijk}.

The lattice size (given by the basis size) is $L = 16$ orbitals and one-site dimension $q = 4$. Thus each ρ_{ij} is a 16 by 16 matrix and each ρ_{ijk} is 64×64. There is exactly 400 nonzero elements of each three-site reduced density matrix ρ_{ijk} and 36 nonzero elements for each ρ_{ij}. Remember that also $i, j, k = 1..16$, which means that there is in total $16^3 \times 400$ relevant matrix elements for the three-site case. Our script in each run calculated one ρ_{ijk} matrix, that means it had to run 400-times. We used a computational cluster with 215 Intel Xeon cores at 3.0 GHz of the J. Heyrovský Institute of Physical Chemistry in Prague.

The resulting two-site mutual information scheme is depicted on graphs in figures 5.3a, 5.4a and 5.4b. The schematic plot of three-site mutual information, which was the main objective to calculate, is on the figure 5.5a. You can see its relative values in table 5.2. For one-site entropy and the eigenvalues of ρ_i, see graphs in figure 5.3b. The one site entropy ρ_i shows how significant is the orbital labelled by i for the chemical bonds, so we can compare it with the rest of the orbitals. In the Attachments section, you can see the plots of two-site hopping amplitudes represented by functions $\langle T^{(u'_i\, u'_j)}_{(u_i\, u_j)} \rangle$.

In the section to follow, we will discuss the observed entanglement pattern and explain how does its structure correspond with the present chemical bonds.

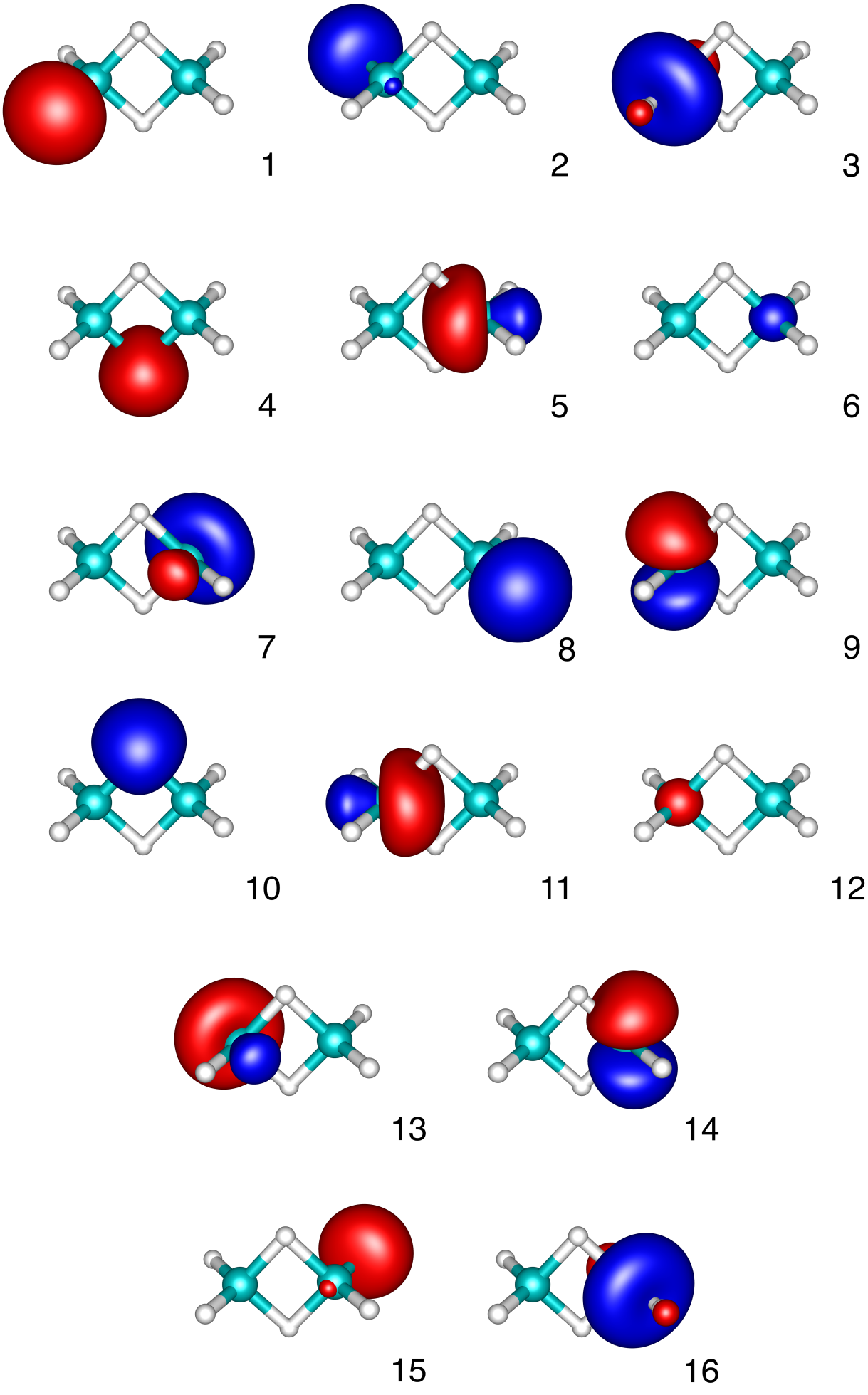

Figure 5.2: Localized (atomic-like) molecular orbitals of diborane.

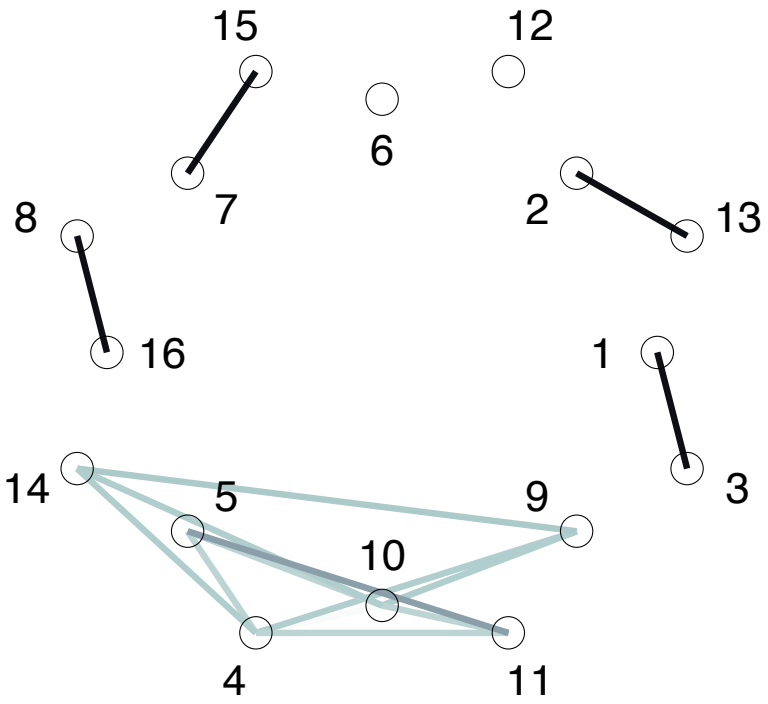

(a) Schematic plot of mutual information I_{ij} for the diborane molecule that we calculated using the QC-DMRG method. Localized (atomic-like) molecular orbitals are labeled by circles and numbered 1..16. See the indexing on figure 5.2. Colour of the lines between the orbitals depict the strength of correlation between them. Darker lines signify higher I_{ij}. For more detailed information on the analysis method, please refer to Szilvási et al. [2015].

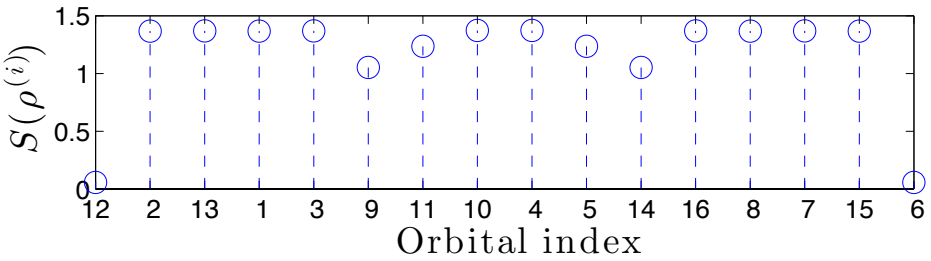

(b) Plot shows the single-orbital entropy $S(\rho_i)$ profile.

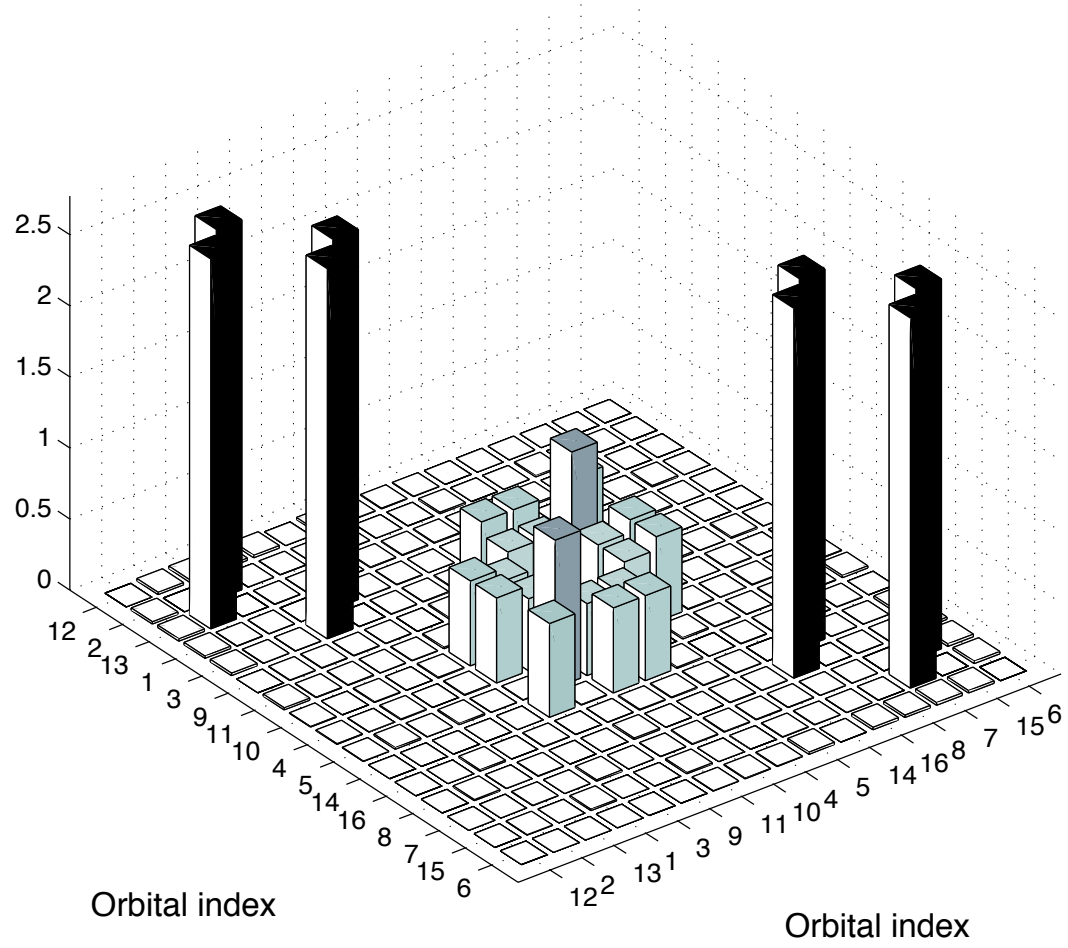

(a) Bar plot of two-site mutual information I_{ij} between the localized (atomic-like) molecular orbitals in the diborane molecule.

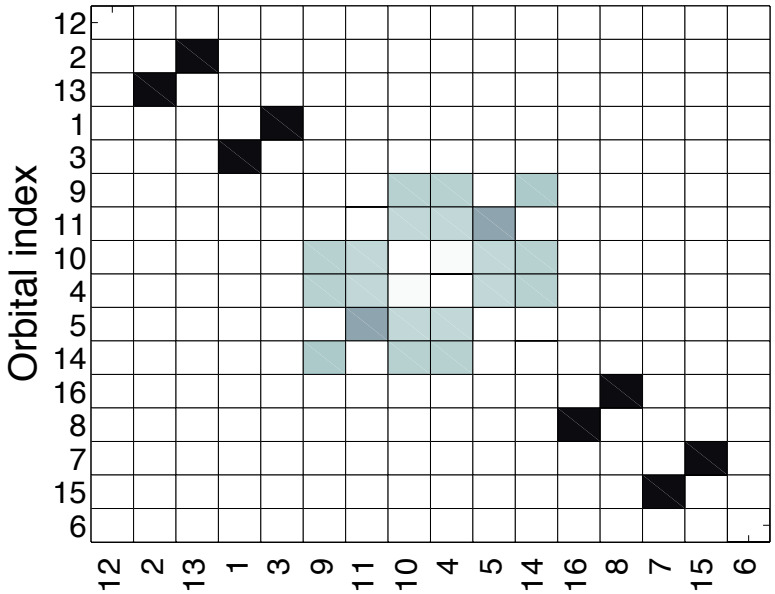

(b) Plot of two-site mutual information I_{ij} between the localized (atomic-like) molecular orbitals in the diborane molecule. Darker squares in the table signify higher values of I_{ij}.

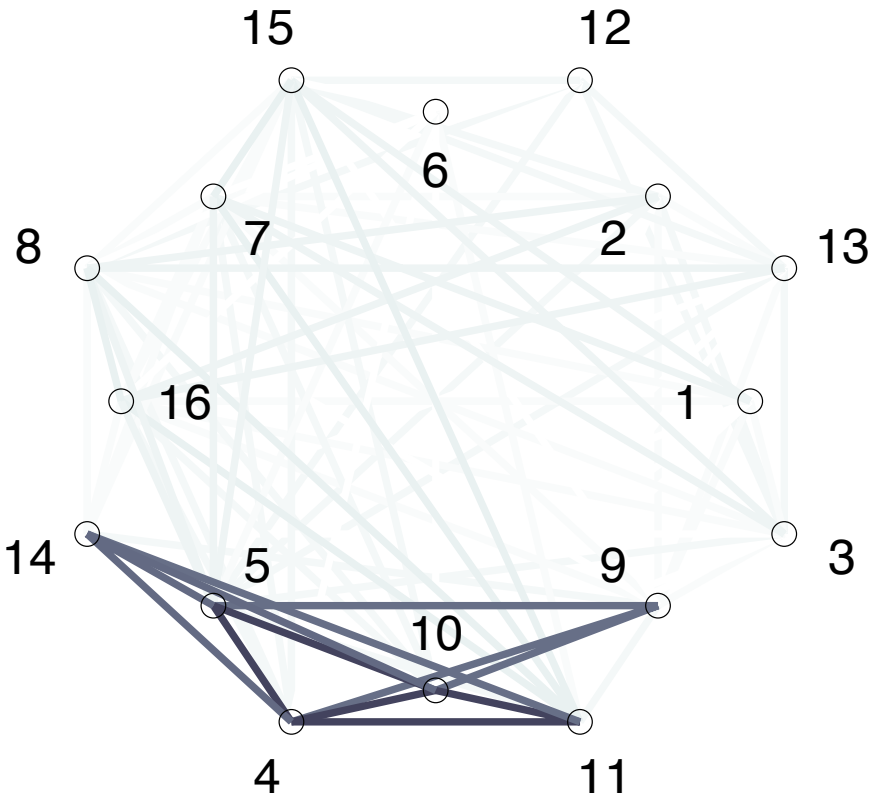

(a) Schematic plot of three-orbital mutual information I_{ijk} for the diborane molecule that we calculated using the QC-DMRG method. Localized (atomic-like) molecular orbitals are labeled by circles and numbered 1..16. See the indexing on figure 5.2. Colour of the lines between the orbitals depict the strength of correlation between them. Darker lines signify higher I_{ijk}. Relative values of I_{ijk} can be found in table 5.2.

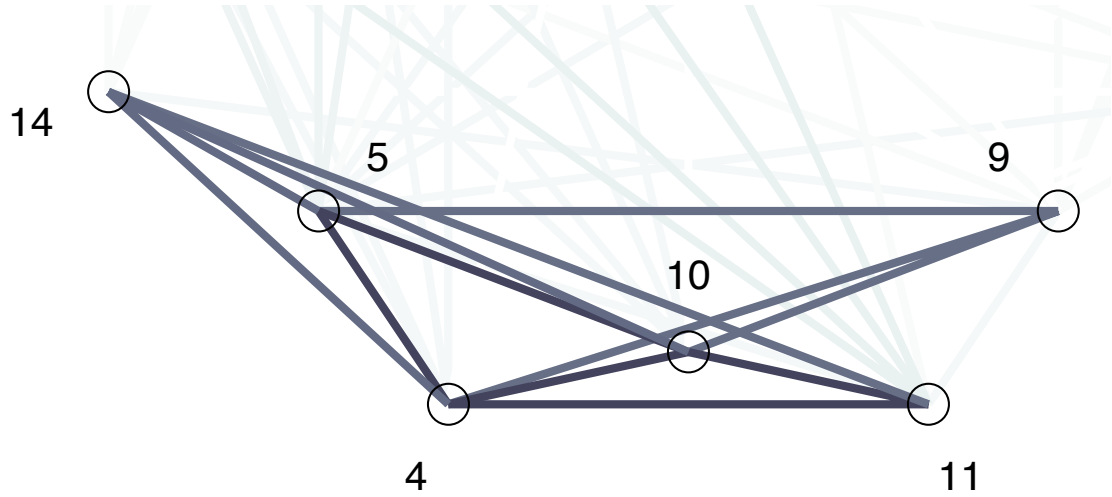

(b) Detail of the 3-orbital 2-electron bonds in the diborane molecule displayed via three-orbital mutual information I_{ijk} plot.

orient.	i-j-k	I_{ijk}	description	orient.	i-j-k	I_{ijk}	description
$> \infty$	4-5-10	0.22	H-B-H hor.	$8 \vee \infty$	4-5-9	0.16	B-H-B mix.
$\infty <$	4-10-11	0.22	H-B-H hor.	$\infty \vee 8$	4-11-14	0.16	B-H-B mix.
$\vee =$	4-5-14	0.17	H=B right	$\infty \wedge 8$	10-11-14	0.16	B-H-B mix.
$\wedge =$	5-10-14	0.17	H=B right	> 8	4-10-14	0.12	H-B-H vert.
$8 \wedge \infty$	5-9-10	0.16	B-H-B mix.	$8 <$	4-9-10	0.12	H-B-H vert.

Table 5.2: Orbital combinations exhibiting the most significant three-site correlation. The values of other combinations are smaller at least by one order of magnitude $I < 0.01$. Horizontal ∞ and vertical 8 in description refers to the spatial orientation of the involved boron orbitals. $\vee$, $\wedge$ correspond to the case which involve the lower and upper hydrogen respectively. For the orientations labelled by $=$, this is a special case when two orbitals of single boron interact with a single hydrogen from the ring. Please don't confuse $=$ with chemical formalism, there is still only one electron involved.

5.5.3 Discussion

Let's start with analysis of the two-site mutual information depicted in figures 5.3a, 5.4a and 5.4b. We can see from the absence of bonds for orbitals 6 and 12 that these core orbitals do not participate, as was expected.

4-covalent σ-bonds between the borons and end hydrogens (outside the ring) are 1-3, 2-13, 7-15, 8-16. These are the strongest detected correlations.

Bonds between orbitals 4, 5, 9, 10, 11 and 14 correspond to the interesting 3 or 4-center bonds.

We can clearly see the bond B-B between boron atoms. This may be due to the correlation of localized orbital with a significant overlap. However, this bond is much weaker than the covalent bond B-H, but still stronger than the 3-center 2-electron bonds. This is in agreement with the fact that the distance between borons is 1.76 Å, while the double of the covalent radius is 1.62 Å. For detailed explanation, please refer to Laszlo [2000].

Considering the two-site mutual information in the 3-center 2-electron bonds in the B_2H_2 ring, in localized orbital basis it looks more like a 4-center 4-electron bonds. This is because the boron orbitals contribute to the bond with both upper and lower half of the ring involved. But this is not a problem from the chemical point of view. If it is so, the H-B-H bonds should also exhibit the three-site correlation and they shouldn't be independent. And this is really the case - we'll see shortly that these are the strongest three-site correlations present in diborane.

According to the single-orbital entropy profile in figure 5.3b, the orbitals are quite equally linked to the rest of the system, with the exceptions in core orbitals 6 and 12, whose contribution is negligible, since the are doubly occupied and hence do not contribute to any other bonds.

Now finally, let's move to the three-site mutual information plot in figure 5.5a. We can happily confirm that the resulting I_{ijk} fully satisfies our hopes to find a significant three-site entanglement in the B_2H_2 ring, between its orbitals 4, 5, 9, 10, 11 and 14. In table 5.2, we compare the I_{ijk} values for the strongest bonds with $0.1 < I_{ijk} < 0.3$. The other bonds outside the ring are at least one order of magnitude weaker, with $I_{ijk} < 0.01$.

The strongest are the H-B-H bonds connected by the horizontal (not vertical!) orbital on the left boron and same for the symmetrical case on the right side. Even though these orbitals are horizontally oriented, they are still large enough to interact with both hydrogens on the ring, thus responsible for what seems as a 4-center 4-electron bond on the two-site plot in figure 5.3a. This is an argument for the hypothesis that the 4-center 4-electron bond is present.

The next on the list ordered by the correlation strength are the odd bonds 4-5-14, 5-10-14 which do not correspond to the case H-B-H, nor B-H-B. Those are the correlations between one hydrogen and two boron orbitals. Their presence is probably caused by the large overlap present and the entanglement inside of the ring, which with a closer look clearly becomes very difficult to describe.

It is obvious from the I_{ijk} plot that the remaining three-site bonds represent the rest of the expected correlation between the overlapping ring orbitals.

Thus we conclude this section with declaring that our expectations were almost fully confirmed and the demonstration of our DMRG module for calculating the three-site entanglement can be considered successful.

Remark. Note that the above three-site mutual information analysis was from some part more intuitive than mathematically rigorous. In some more delicate cases than this simple demonstration, we have to be aware of the complications that may arise with nonintuitive behaviour of definitions, with properties of multipartite mutual information or with the linked quantities. For further reading from a mathematical point of view, please refer to Williams and Beer [2010] and Szalay et al. [2016]. A rigorous description of the multipartite entanglement measures is beyond reach of this thesis.

Conclusion and Outlook

5.6 Conlusion

We have made a module for calculating the three-site operator correlations in the Budapest implementation of the Density Matrix Renormalization Method.

We have sucessfully calculated the three-site mutual information for diborane and we used it together with other corresponding quantities to analyze the entanglement pattern. We discussed the results extensively in the last chapter, concluding a successful verification of the theoretical prediction of the outcomes. We have verified the presence of three-partite mutual information in the B_2H_2 ring in the diborane molecule.

In the theoretical part, we introduced the relevant terms to build a basic quantum information theoretical picture about the problem. We have reviewed serveral methods for optimizing the of the quantum simulations, namely for the DMRG method.

Bibliography

G. Barcza, R. M. Noack, J. Sólyom, and Ö. Legeza. Entanglement patterns and generalized correlation functions in quantum many-body systems. *Phys. Rev. B*, 92:125140, Sep 2015. doi: 10.1103/PhysRevB.92.125140. URL `http://link.aps.org/doi/10.1103/PhysRevB.92.125140`.

John S. Bell. On the Einstein-Podolsky-Rosen paradox. *Physics*, 1:195–200, 1964.

Charles H Bennett. Quantum information. *Physica Scripta*, 1998(T76):210, 1998. URL `http://stacks.iop.org/1402-4896/1998/i=T76/a=030`.

Dik Bouwmeester, Jian-Wei Pan, Matthew Daniell, Harald Weinfurter, and Anton Zeilinger. Observation of three-photon greenberger-horne-zeilinger entanglement. *Phys. Rev. Lett.*, 82:1345–1349, Feb 1999. doi: 10.1103/PhysRevLett.82.1345. URL `http://link.aps.org/doi/10.1103/PhysRevLett.82.1345`.

M. Chandross and J. C. Hicks. Density-matrix renormalization-group method for excited states. *Phys. Rev. B*, 59:9699–9702, Apr 1999. doi: 10.1103/PhysRevB.59.9699. URL `http://link.aps.org/doi/10.1103/PhysRevB.59.9699`.

M. Crouzeix, B. Philippe, and M. Sadkane. The davidson method. *SIAM J. Sci. Comput.*, 15(1):62–76, January 1994. ISSN 1064-8275. doi: 10.1137/0915004. URL `http://dx.doi.org/10.1137/0915004`.

Victor Eijkhout. Lapack working note 50 distributed sparse data structures for linear algebra operations, 1992.

A. Einstein, B. Podolsky, and N. Rosen. Can quantum-mechanical description of physical reality be considered complete? *Phys. Rev.*, 47:777–780, May 1935. doi: 10.1103/PhysRev.47.777. URL `http://link.aps.org/doi/10.1103/PhysRev.47.777`.

A. Galindo and M. A. Martín-Delgado. Information and computation: Classical and quantum aspects. *Rev. Mod. Phys.*, 74:347–423, May 2002. doi: 10.1103/RevModPhys.74.347. URL `http://link.aps.org/doi/10.1103/RevModPhys.74.347`.

Prof. Walter Gander. The singular value decomposition, December 2008. URL `https://www.math.muni.cz/~zelinka/cjh/svd.pdf`. Innotec lecture notes.

Gene H. Golub and Charles F. Van Loan. *Matrix Computations (3rd Ed.)*. Johns Hopkins University Press, Baltimore, MD, USA, 1996. ISBN 0-8018-5414-8.

Daniel M. Greenberger, Michael A. Horne, and Anton Zeilinger. *Going Beyond Bell's Theorem*, pages 69–72. Springer Netherlands, Dordrecht, 1989. ISBN 978-94-017-0849-4. doi: 10.1007/978-94-017-0849-4_10. URL http://dx.doi.org/10.1007/978-94-017-0849-4_10.

L. P. Kadanoff. Scaling laws for Ising models near T(c). *Physics*, 2:263–272, 1966.

Pierre Laszlo. A diborane story. *Angewandte Chemie International Edition*, 39(12):2071–2072, 2000. ISSN 1521-3773. doi: 10.1002/1521-3773(20000616)39:12⟨2071::AID-ANIE2071⟩3.0.CO;2-C. URL http://dx.doi.org/10.1002/1521-3773(20000616)39:12<2071::AID-ANIE2071>3.0.CO;2-C.

Ö. Legeza and J. Sólyom. Optimizing the density-matrix renormalization group method using quantum information entropy. *Phys. Rev. B*, 68:195116, Nov 2003. doi: 10.1103/PhysRevB.68.195116. URL http://link.aps.org/doi/10.1103/PhysRevB.68.195116.

Ö. Legeza, J. Röder, and B. A. Hess. Controlling the accuracy of the density-matrix renormalization-group method: The dynamical block state selection approach. *Phys. Rev. B*, 67:125114, Mar 2003. doi: 10.1103/PhysRevB.67.125114. URL http://link.aps.org/doi/10.1103/PhysRevB.67.125114.

Ö. Legeza, R.M. Noack, J. Sólyom, and L. Tincani. *Applications of Quantum Information in the Density-Matrix Renormalization Group*, pages 653–664. Springer Berlin Heidelberg, Berlin, Heidelberg, 2008. ISBN 978-3-540-74686-7. doi: 10.1007/978-3-540-74686-7_24. URL http://dx.doi.org/10.1007/978-3-540-74686-7_24.

Gerrit Moritz and Markus Reiher. Construction of environment states in quantum-chemical density-matrix renormalization group calculations. *The Journal of Chemical Physics*, 124(3):034103, 2006. doi: http://dx.doi.org/10.1063/1.2139998. URL http://scitation.aip.org/content/aip/journal/jcp/124/3/10.1063/1.2139998.

V. Murg, F. Verstraete, Ö. Legeza, and R. M. Noack. Simulating strongly correlated quantum systems with tree tensor networks. *Phys. Rev. B*, 82:205105, Nov 2010. doi: 10.1103/PhysRevB.82.205105. URL http://link.aps.org/doi/10.1103/PhysRevB.82.205105.

Naoki Nakatani and Garnet Kin-Lic Chan. Efficient tree tensor network states (ttns) for quantum chemistry: Generalizations of the density matrix renormalization group algorithm. *The Journal of Chemical Physics*, 138(13):134113, 2013. doi: http://dx.doi.org/10.1063/1.4798639. URL http://scitation.aip.org/content/aip/journal/jcp/138/13/10.1063/1.4798639.

Roman F. Nalewajski. Entropy descriptors of the chemical bond in information theory. i. basic concepts and relations. *Molecular Physics*, 102(6):531–546, 2004. doi: 10.1080/00268970410001675581. URL http://dx.doi.org/10.1080/00268970410001675581.

Ulrich Schollwöck. The density-matrix renormalization group in the age of matrix product states. *Annals of Physics*, 326(1):96 – 192, 2011. ISSN 0003-4916. doi: http://dx.doi.org/10.1016/j.aop.2010.09.012. URL http://www.sciencedirect.com/science/article/pii/S0003491610001752. January 2011 Special Issue.

E. Schrödinger. Die gegenwärtige situation in der quantenmechanik. *Naturwissenschaften*, 23(48):807–812, 1935. ISSN 1432-1904. doi: 10.1007/BF01491891. URL http://dx.doi.org/10.1007/BF01491891.

Gaurav Sharma and Jos Martin. Matlab®: A language for parallel computing. *International Journal of Parallel Programming*, 37(1):3–36, 2009. ISSN 1573-7640. doi: 10.1007/s10766-008-0082-5. URL http://dx.doi.org/10.1007/s10766-008-0082-5.

S. Szalay, G. Barcza, T. Szilvási, L. Veis, and Ö. Legeza. The correlation theory of the chemical bond. *ArXiv e-prints*, May 2016.

Szilárd Szalay, Max Pfeffer, Valentin Murg, Gergely Barcza, Frank Verstraete, Reinhold Schneider, and Örs Legeza. Tensor product methods and entanglement optimization for ab initio quantum chemistry. *International Journal of Quantum Chemistry*, 115(19):1342–1391, 2015. ISSN 1097-461X. doi: 10.1002/qua.24898. URL http://dx.doi.org/10.1002/qua.24898.

T. Szilvási, G. Barcza, and Ö. Legeza. Concept of chemical bond and aromaticity based on quantum information theory. *ArXiv e-prints*, September 2015.

The MathWorks, Inc. Matlab compiler, July 2016a. URL http://www.mathworks.com/help/compiler/.

The MathWorks, Inc. Matlab parallel computing toolbox, July 2016b. URL http://www.mathworks.com/help/distcomp/.

H-JKPJ Werner, PJ Knowles, G Knizia, FR Manby, M Schütz, P Celani, T Korona, R Lindh, A Mitrushenkov, G Rauhut, et al. Molpro, version 2010.1, a package of ab initio programs. *See http://www. molpro. net*, 2010.

S. R. White and R. M. Noack. Real-space quantum renormalization groups. *Phys. Rev. Lett.*, 68:3487–3490, Jun 1992. doi: 10.1103/PhysRevLett.68.3487. URL http://link.aps.org/doi/10.1103/PhysRevLett.68.3487.

Steven R. White. Density matrix formulation for quantum renormalization groups. *Phys. Rev. Lett.*, 69:2863–2866, Nov 1992. doi: 10.1103/PhysRevLett.69.2863. URL http://link.aps.org/doi/10.1103/PhysRevLett.69.2863.

Steven R. White. Density-matrix algorithms for quantum renormalization groups. *Phys. Rev. B*, 48:10345–10356, Oct 1993. doi: 10.1103/PhysRevB.48.10345. URL http://link.aps.org/doi/10.1103/PhysRevB.48.10345.

Wikimedia Commons. Diborane molecule scheme, July 2016. URL https://en.wikipedia.org/wiki/File:Diborane-2D.png.

Paul L. Williams and Randall D. Beer. Nonnegative decomposition of multivariate information. *CoRR*, abs/1004.2515, 2010. URL http://arxiv.org/abs/1004.2515.

Kenneth G. Wilson. The renormalization group: Critical phenomena and the kondo problem. *Rev. Mod. Phys.*, 47:773–840, Oct 1975. doi: 10.1103/RevModPhys.47.773. URL http://link.aps.org/doi/10.1103/RevModPhys.47.773.

Sebastian Wouters, Thomas Bogaerts, Pascal Van Der Voort, Veronique Van Speybroeck, and Dimitri Van Neck. Communication: Dmrg-scf study of the singlet, triplet, and quintet states of oxo-mn(salen). *The Journal of Chemical Physics*, 140(24):241103, 2014. doi: http://dx.doi.org/10.1063/1.4885815. URL http://scitation.aip.org/content/aip/journal/jcp/140/24/10.1063/1.4885815.

List of Figures

List of Tables

List of Abbreviations

Attachments

Attachment 1: Following pages contain graphs of all the 36 two-site generalized correlations functions for the diborane molecule.

$T_i^{(1)} \times T_j^{(1)} : -_i,-_j \implies -_i,-_j : \rho_{i,j}(1,1)$

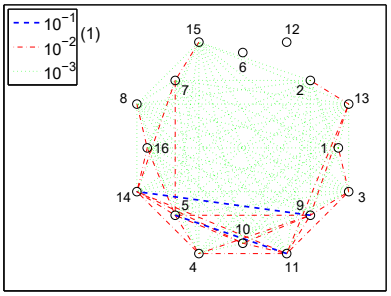

$T_i^{(1)} \times T_j^{(6)} : -_i,\downarrow_j \implies -_i,\downarrow_j : \rho_{i,j}(2,2)$

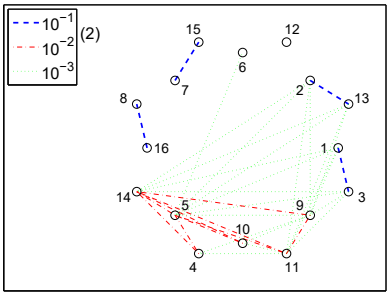

$T_i^{(1)} \times T_j^{(11)} : -_i,\uparrow_j \implies -_i,\uparrow_j : \rho_{i,j}(3,3)$

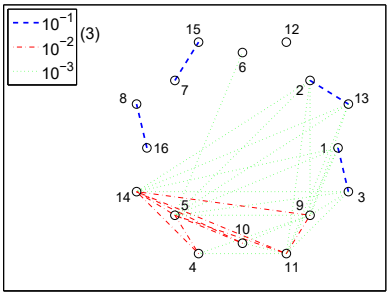

$T_i^{(1)} \times T_j^{(16)} : -_i,\uparrow\downarrow_j \implies -_i,\uparrow\downarrow_j : \rho_{i,j}(4,4)$

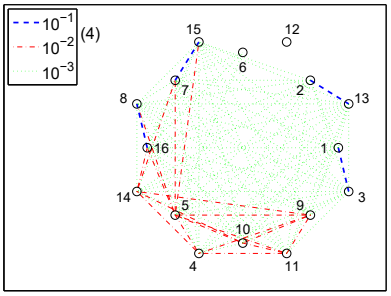

$T_i^{(2)} \times T_j^{(5)} : \downarrow_i,-_j \implies -_i,\downarrow_j : \rho_{i,j}(2,5)$

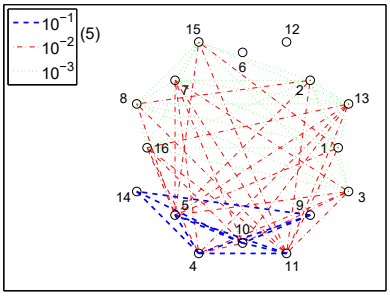

$T_i^{(2)} \times T_j^{(15)} : \downarrow_i,\uparrow_j \implies -_i,\uparrow\downarrow_j : \rho_{i,j}(4,7)$

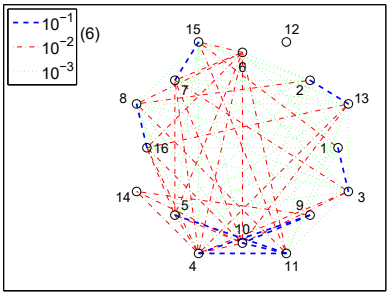

$T_i^{(3)} \times T_j^{(9)} : \uparrow_i,-_j \implies -_i,\uparrow_j : \rho_{i,j}(3,9)$

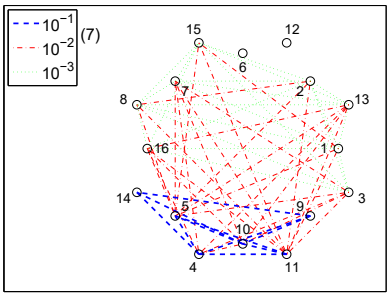

$T_i^{(3)} \times T_j^{(14)} : \uparrow_i,\downarrow_j \implies -_i,\uparrow\downarrow_j : \rho_{i,j}(4,10)$

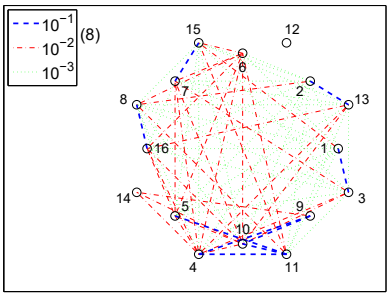

$T_i^{(4)} \times T_j^{(13)} : \uparrow\downarrow_i,-_j \implies -_i,\uparrow\downarrow_j : \rho_{i,j}(4,13)$

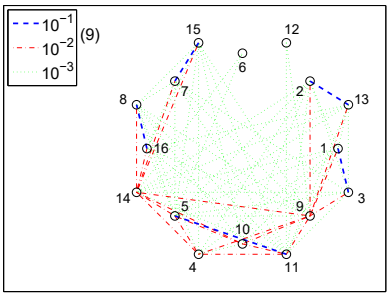

$T_i^{(5)} \times T_j^{(2)} : -_i,\downarrow_j \implies \downarrow_i,-_j : \rho_{i,j}(5,2)$

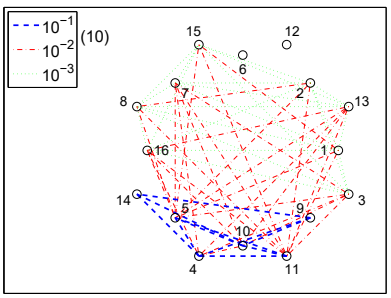

$T_i^{(5)} \times T_j^{(12)} : -_i,\uparrow\downarrow_j \implies \downarrow_i,\uparrow_j : \rho_{i,j}(7,4)$

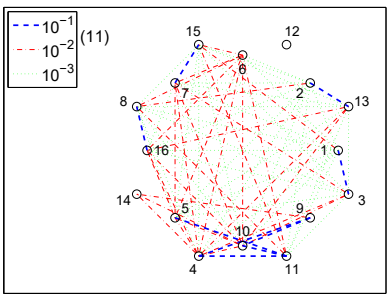

$T_i^{(6)} \times T_j^{(1)} : \downarrow_i,-_j \implies \downarrow_i,-_j : \rho_{i,j}(5,5)$

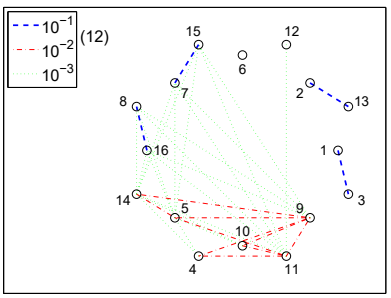

$T_i^{(6)} \times T_j^{(6)} : \downarrow_i,\downarrow_j \implies \downarrow_i,\downarrow_j : \rho_{i,j}(6,6)$

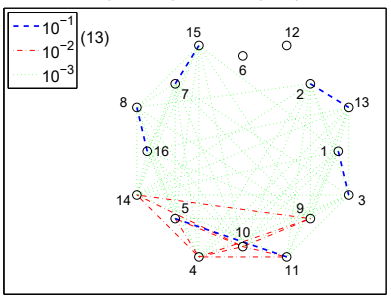

$T_i^{(6)} \times T_j^{(11)} : \downarrow_i,\uparrow_j \implies \downarrow_i,\uparrow_j : \rho_{i,j}(7,7)$

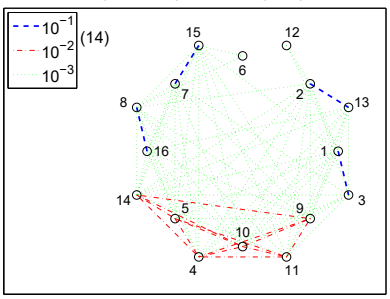

$T_i^{(6)} \times T_j^{(16)} : \downarrow_i,\uparrow\downarrow_j \implies \downarrow_i,\uparrow\downarrow_j : \rho_{i,j}(8,8)$

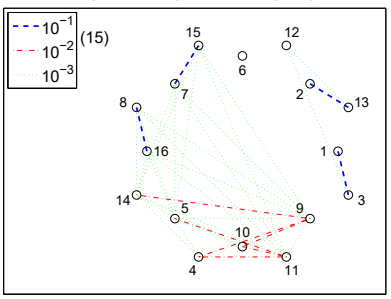

$T_i^{(7)} \times T_j^{(10)} : \uparrow_i,\downarrow_j \implies \downarrow_i,\uparrow_j : \rho_{i,j}(7,10)$

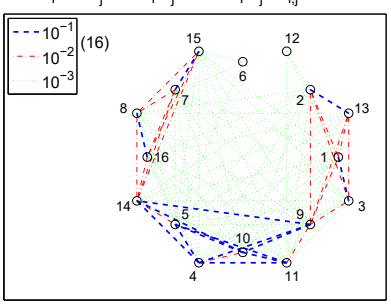

$T_i^{(8)} \times T_j^{(9)} : \uparrow\downarrow_i,-_j \implies \downarrow_i,\uparrow_j : \rho_{i,j}(7,13)$

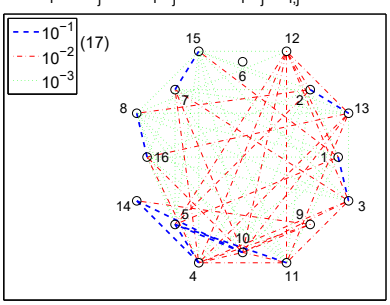

$T_i^{(8)} \times T_j^{(14)} : \uparrow\downarrow_i,\downarrow_j \implies \downarrow_i,\uparrow\downarrow_j : \rho_{i,j}(8,14)$

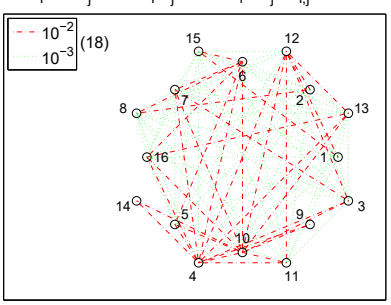

$T_i^{(9)} \times T_j^{(3)} : -_i,\uparrow_j \implies \uparrow_i,-_j : \rho_{i,j}(9,3)$

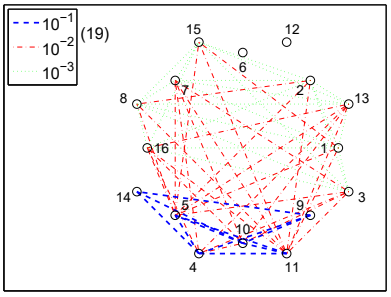

$T_i^{(9)} \times T_j^{(8)} : -_i,\uparrow\downarrow_j \implies \uparrow_i,\downarrow_j : \rho_{i,j}(10,4)$

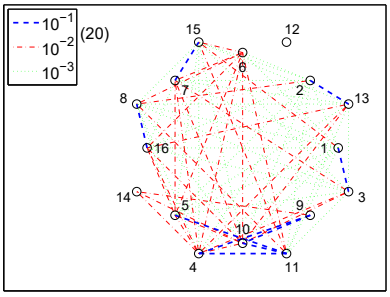

$T_i^{(10)} \times T_j^{(7)} : \downarrow_i,\uparrow_j \implies \uparrow_i,\downarrow_j : \rho_{i,j}(10,7)$

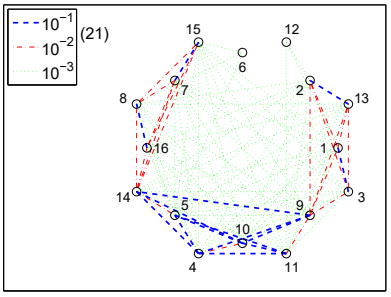

$T_i^{(11)} \times T_j^{(1)} : \uparrow_i,-_j \implies \uparrow_i,-_j : \rho_{i,j}(9,9)$

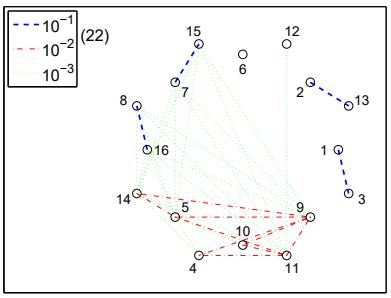

$T_i^{(11)} \times T_j^{(6)} : \uparrow_i,\downarrow_j \implies \uparrow_i,\downarrow_j : \rho_{i,j}(10,10)$

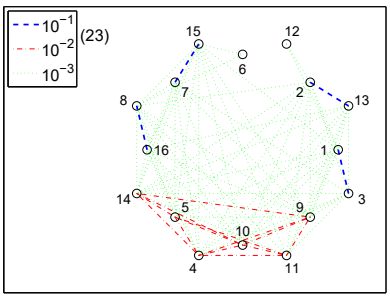

$T_i^{(11)} \times T_j^{(11)} : \uparrow_i,\uparrow_j \implies \uparrow_i,\uparrow_j : \rho_{i,j}(11,11)$

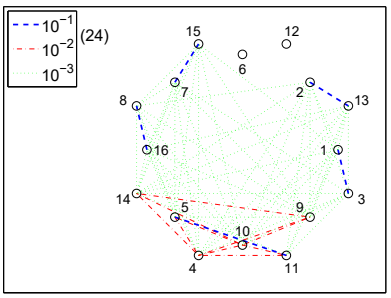

$T_i^{(11)} \times T_j^{(16)} : \uparrow_i,\uparrow\downarrow_j \implies \uparrow_i,\uparrow\downarrow_j : \rho_{i,j}(12,12)$

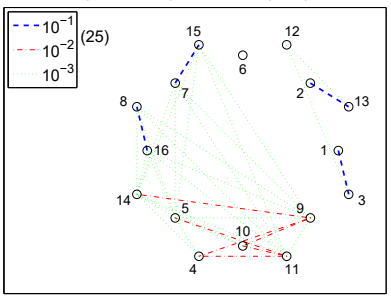

$T_i^{(12)} \times T_j^{(5)} : \uparrow\downarrow_i,-_j \implies \uparrow_i,\downarrow_j : \rho_{i,j}(10,13)$

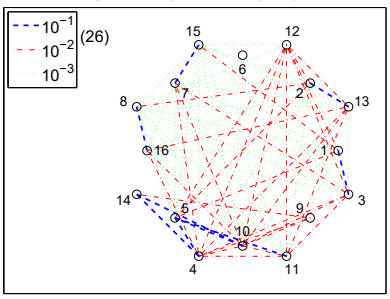

$T_i^{(12)} \times T_j^{(15)} : \uparrow\downarrow_i,\uparrow_j \implies \uparrow_i,\uparrow\downarrow_j : \rho_{i,j}(12,15)$

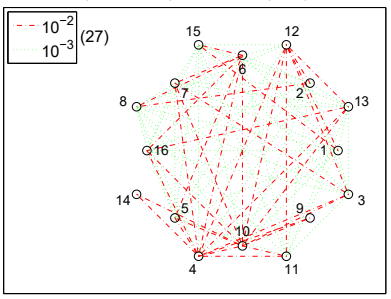

$T_i^{(13)} \times T_j^{(4)} : -_i,\uparrow\downarrow_j \implies \uparrow\downarrow_i,-_j : \rho_{i,j}(13,4)$

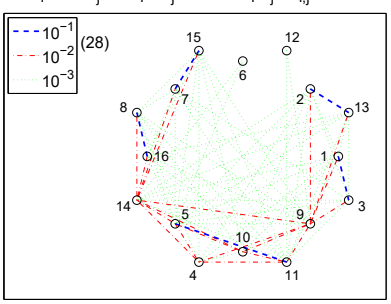

$T_i^{(14)} \times T_j^{(3)} : \downarrow_i,\uparrow_j \implies \uparrow\downarrow_i,-_j : \rho_{i,j}(13,7)$

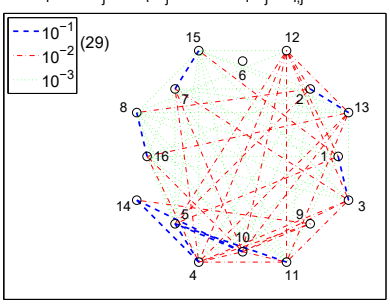

$T_i^{(14)} \times T_j^{(8)} : \downarrow_i,\uparrow\downarrow_j \implies \uparrow\downarrow_i,\downarrow_j : \rho_{i,j}(14,8)$

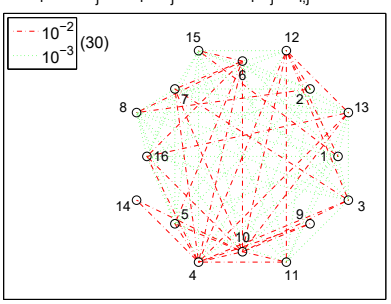

$T_i^{(15)} \times T_j^{(2)} : \uparrow_i,\downarrow_j \implies \uparrow\downarrow_i,-_j : \rho_{i,j}(13,10)$

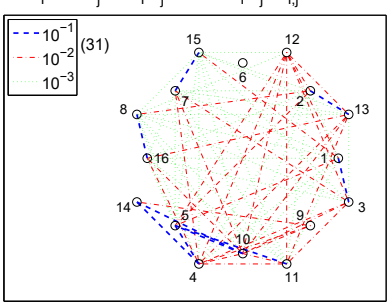

$T_i^{(15)} \times T_j^{(12)} : \uparrow_i,\uparrow\downarrow_j \implies \uparrow\downarrow_i,\uparrow_j : \rho_{i,j}(15,12)$

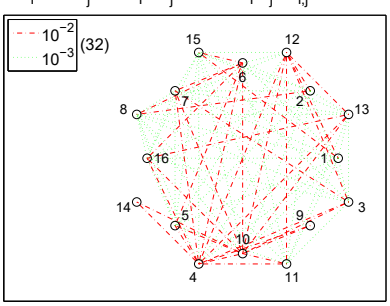

$T_i^{(16)} \times T_j^{(1)} : \uparrow\downarrow_i,-_j \implies \uparrow\downarrow_i,-_j : \rho_{i,j}(13,13)$

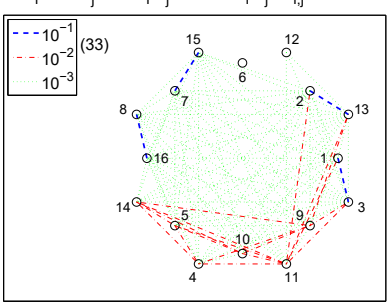

$T_i^{(16)} \times T_j^{(6)} : \uparrow\downarrow_i,\downarrow_j \implies \uparrow\downarrow_i,\downarrow_j : \rho_{i,j}(14,14)$

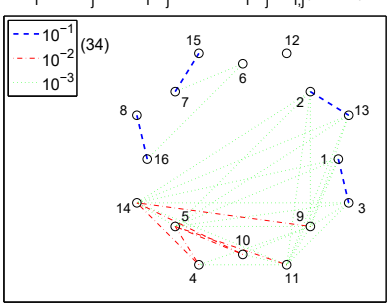

$T_i^{(16)} \times T_j^{(11)} : \uparrow\downarrow_i,\uparrow_j \implies \uparrow\downarrow_i,\uparrow_j : \rho_{i,j}(15,15)$

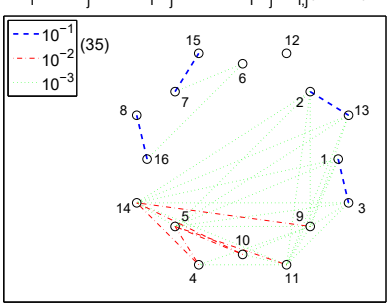

$T_i^{(16)} \times T_j^{(16)} : \uparrow\downarrow_i,\uparrow\downarrow_j \implies \uparrow\downarrow_i,\uparrow\downarrow_j : \rho_{i,j}(16,16)$